



AMERICAN UNIVERSITY OF BEIRUT

TWO NOVEL LOW ENERGY  
MECHANICALLY RECONFIGURABLE  
ANTENNAS BASED ON CHLADNI AND  
MOIRE PATTERNS

by  
JOE ELIAS TAOUM

A thesis  
submitted in partial fulfillment of the requirements  
for the degree of Master of Engineering  
to the Department of Mechanical Engineering  
of the Maroun Semaan Faculty of Engineering and Architecture  
at the American University of Beirut

Beirut, Lebanon  
June 2021

AMERICAN UNIVERSITY OF BEIRUT

TWO NOVEL LOW ENERGY  
MECHANICALLY RECONFIGURABLE  
ANTENNAS BASED ON CHLADNI AND  
MOIRE PATTERNS

by  
JOE ELIAS TAOUM

Approved by:

Dr. Elie Shammas, Associate Professor  
Mechanical Engineering

Advisor



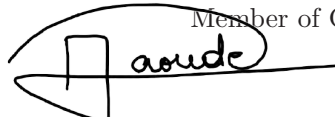
Dr. Joseph Costantine, Associate Professor  
Electrical and Computer Engineering

Co-Advisor



Dr. Dany Abou Jaoude, Assistant Professor  
Mechanical Engineering

Member of Committee



Dr. Youssef Tawk, Assistant Professor  
Electrical and Computer Engineering

Member of Committee



Date of thesis: June 10, 2021

# AMERICAN UNIVERSITY OF BEIRUT

## THESIS, DISSERTATION, PROJECT RELEASE FORM

Student Name: Taoum Joe Elias  
Last First Middle

Master's Thesis       Master's Project       Doctoral Dissertation

I authorize the American University of Beirut to: (a) reproduce hard or electronic copies of my thesis, dissertation, or project; (b) include such copies in the archives and digital repositories of the University; and (c) make freely available such copies to third parties for research or educational purposes.

I authorize the American University of Beirut, to: (a) reproduce hard or electronic copies of it; (b) include such copies in the archives and digital repositories of the University; and (c) make freely available such copies to third parties for research or educational purposes after: **One \_\_\_ year from the date of submission of my thesis, dissertation or project.**  
**Two \_\_\_ years from the date of submission of my thesis , dissertation or project.**  
**Three  years from the date of submission of my thesis , dissertation or project.**



Signature

June 10, 2021

Date

This form is signed when submitting the thesis, dissertation, or project to the University Libraries

# Acknowledgements

I would first like to thank my main advisor Dr. Elie Shammas and my co-advisor Dr. Joseph Costantine for guiding me throughout this work. Both professors always steered me in the right direction despite the many barriers that encountered me during this journey.

I would also like to thank the American University of Beirut for providing me with a supportive environment to be able to complete my work. The prototypes and experimental testing would not have been possible without the equipment provided by the departments of mechanical engineering and electrical and computer engineering. A special thank you also goes to Dr. Hassan Shwaykani and Dr. Fatima Alzahraa Asadallah for their continuous assistance.

I would also like to acknowledge Dr. Dany Abou Jaoude and Dr. Youssef Tawk for being members of my thesis committee and for their valuable comments.

Finally, I must express my forever gratitude to my parents, my siblings, my grandmother and my dearest friends Marianne and Sabine for providing me with unmatched support and endless motivation throughout my years of study. Nothing would have been possible without you. I cannot thank you enough.

# An Abstract of the Thesis of

Joe Elias Taoum for Master of Engineering  
Major: Mechanical Engineering

Title: Two Novel Low Energy Mechanically Reconfigurable Antennas based on Chladni and Moire Patterns

In this thesis, two mechanically reconfigurable antennas are proposed. The first antenna is based on the moiré phenomenon, where the relative rotation of two superposed layers produces new topologies. The two patches are circular, fabricated on an FR4 substrate with a layer of copper. The patterns are horizontal lines milled into the substrate. The actuation mechanism relies on a ratchet mechanism and is actuated by a shape memory alloy (SMA) spring. The simulations and measurement of the fabricated prototype show polarization reconfiguraton, along with a beam focusing effect at high rotation angles. The second design concept relies on the vibration of conductive grains on top of a patch antenna to create different patterns. These shapes of the standing waves, known as Chladni patterns, are obtained by exciting a thin plate at different frequencies. The effect of these patterns on the antenna characteristics depends on several factors that still need to be investigated and analyzed.

# Contents

<b>Acknowledgements</b>	<b>v</b>
<b>Abstract</b>	<b>vi</b>
<b>1 Introduction</b>	<b>1</b>
<b>2 Literature Review</b>	<b>6</b>
<b>3 Moiré Patterns Antenna</b>	<b>11</b>
3.1 Background . . . . .	11
3.2 Working Principle . . . . .	13
3.3 Mechanical Design . . . . .	16
3.3.1 Moiré Circular Patches . . . . .	17
3.3.2 SMA Actuator . . . . .	19
3.3.3 Ratchet Mechanism . . . . .	20
3.3.4 Previous Designs . . . . .	23
3.4 Simulations and Experimental Results . . . . .	24
<b>4 Chladni Patterns Antenna</b>	<b>29</b>
4.1 Background . . . . .	29
4.2 Mechanical Design . . . . .	31
4.2.1 FR4 Substrate . . . . .	32
4.2.2 Conductive Grains . . . . .	33
4.2.3 Actuators . . . . .	36
4.3 Simulations and Experimental Results . . . . .	37
<b>5 Future Work</b>	<b>49</b>
5.1 Moiré Patterns Antenna . . . . .	49
5.2 Chladni Patterns Antenna . . . . .	49

# List of Figures

1.1	Common types of antennas [2]. . . . .	2
1.2	Omnidirectional vs directional radiation patterns [1]. . . . .	3
1.3	Example of polarization patterns [4]. . . . .	4
1.4	Frequency and bandwidth reconfiguration example [7]. . . . .	4
1.5	Beam steering example[8]. . . . .	5
2.1	A frequency reconfigurable monopole using soft robotics [12]. . . . .	7
2.2	Beam steering reconfigurable antenna using liquid metal director and reflector [16]. . . . .	8
2.3	CP patch antenna design. . . . .	10
3.1	Typical examples of moiré stacking [33]. . . . .	11
3.2	Moiré pattern in document counterfeit [35]. . . . .	12
3.3	Simplified illustrations of the working principle of the proposed antenna seen as (a) a top view, (b) a perspective view, and (c) an exploded view. . . . .	14
3.4	Moiré patterns obtained by rotating two circular patches with a copper layer by (a) 0 deg, (b) 10 deg, and (c) 30 deg. . . . .	14
3.5	Simulated surface current distribution on the moiré patches at (a) 0 deg rotation, (b) 10 deg rotation, and (c) 30 deg rotation. . . . .	15
3.6	CAD representation of the proposed reconfigurable antenna seen as (a) a top view along its cross-sectional view, (b) an exploded view. . . . .	16
3.7	Moiré patches made from one sided copper FR4 substrate. . . . .	17
3.8	Moiré effect by rotating the teethed disc. . . . .	18
3.9	CAD representation of the proposed actuation mechanism as (a) a top view, (b) an annotated perspective view. . . . .	20
3.10	Actuation mechanism used in the prototype. . . . .	21
3.11	CAD representation of the proposed actuation mechanism as (a) a top view, (b) an annotated perspective view. . . . .	22
3.12	Previous fabricated prototypes. . . . .	23
3.13	Fabricated antenna prototype. . . . .	24
3.14	Simulated and measured S11 of the proposed antenna. . . . .	25



3.15	Simulated radiation patterns at (a) 0 deg rotation, (b) 10 deg rotation, and (c) 30 deg rotation. . . . .	26
3.16	Normalized simulated and measured radiation patterns of the dominant components at (a) 0 deg rotation, (b) 10 deg rotation, and (c)(d) 30 deg rotation. . . . .	27
3.17	Three-dimensional realized gain patterns at (a) 0 deg, (b) 10 deg, and (c) 30 deg rotations, respectively. . . . .	27
3.18	Axial ratio of the proposed antenna at 30 deg (a) throughout its S11 bandwidth, and (b) at 2.56 GHz. . . . .	28
4.1	Patterns obtained by Ernst Chladni in 1787 [44]. . . . .	30
4.2	Chladni patterns obtained using copper filings. . . . .	31
4.3	Main components of the Chladni patterns antenna. . . . .	32
4.4	Shape and size comparison of plastic sheets. . . . .	34
4.5	Copper powder shape benchmark. . . . .	35
4.6	Comparing the results of the patterns using plastic sheets Vs Aluminum foil. . . . .	35
4.7	Types of haptic actuators with relevant applications. . . . .	36
4.8	Vibration setup. . . . .	38
4.9	Steps to simulate experimental Chladni patterns . . . . .	38
4.10	S11 of the Simulated Antenna With and Without Foil . . . . .	39
4.11	Gain of the simulated antenna with and without foil. . . . .	39
4.12	FR4 plate model for harmonic response simulations. . . . .	42
4.13	Frequency response of two actuator configurations. . . . .	42
4.14	Modal shapes comparison for two different actuator placement . .	43
4.15	Harmonic response simulation of the plate on the vibration exciter setup. . . . .	44
4.16	Harmonic response simulation of the different plate shapes. . . . .	45
4.17	Frequency response of two actuator configurations. . . . .	46
4.18	Simulated offset shapes of circular plates. . . . .	46
4.19	Radiation patterns of the simulated offset shapes. . . . .	47
4.20	S11 plot of the simulated offset shapes. . . . .	48

# Chapter 1

## Introduction

In a world governed by wireless devices, great interest in antenna design has emerged in both the industry and research community. Whether for data transfer, wireless telemetry, internet, or phone and satellite communications, antennas are considered vital components in modern days electronics. By definition, an antenna is a structure capable of transmitting or receiving radio frequency (RF) signals [1]. These structures, usually of metallic nature, come in different forms and shapes. The different types of antennas include wire antennas (dipole, loop and helix), aperture antennas, microstrip antennas, array antennas and reflector antennas [2]. Figure 1.1 illustrates different examples of the mentioned antennas.

The main objective behind having different types of antennas is to satisfy certain requirements of the antenna's operation properties. These requirements are translated into a set of characteristics, or parameters, imposed by the antenna design. Some of the fundamental parameters of an antenna are [3]:

- Radiation pattern.
- Radiation intensity.
- Beamwidth.
- Directivity and gain.
- Polarization.
- Bandwidth.
- Effective length.

Although having a lossless isotropic antenna is only theoretical, we can classify the radiation patterns emitted by an antenna as either directional or omnidirectional. Figure 1.2 illustrates the difference between an omnidirectional radiation pattern of a monopole, and a very directional beam emitted by a horn antenna, where a major lobe clearly favors a certain direction and not the others [1].

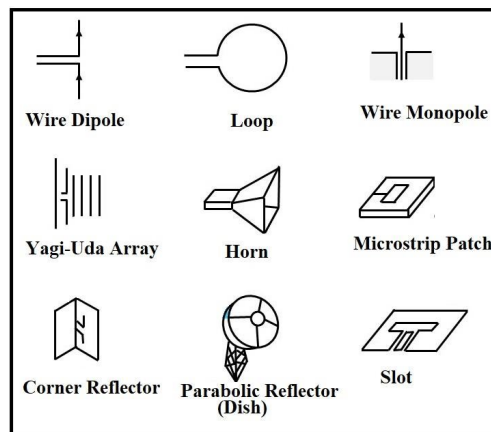
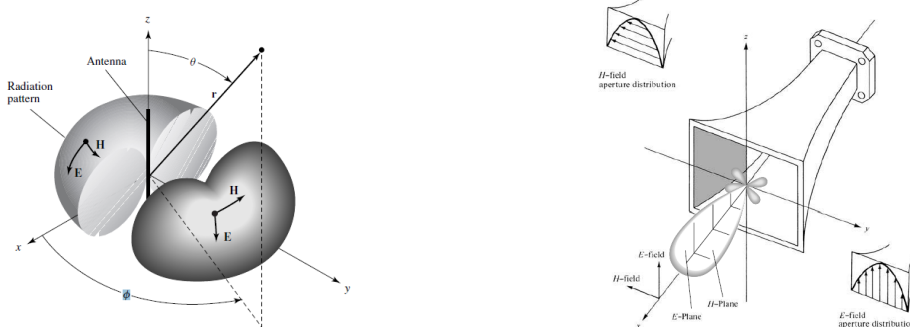


Figure 1.1: Common types of antennas [2].

Depending on the direction of travel of the electric field of the radiated wave, an antenna's polarization can be classified as either linear, circular, or elliptical, as shown in figure 1.3. In the most general case, a wave travels in an elliptical profile. However, if the ellipse is restricted to a line, which indicates that the electric field's vector travels in a single plane containing the direction of propagation, then the polarizing is linear. On the other hand, if the ellipse becomes a circle, the polarization is said to be circular. Another important aspect of the travelling wave is its rotational direction: a clockwise (CW) rotation is referred to as right-hand polarization; whereas a counterclockwise (CCW) rotation are called left-hand polarization [1].

Despite the fact that conventional methods to communicate in multiple frequencies or switching radiation patterns require having many antennas with different characteristics, researchers have been exploring the idea of reconfigurable antennas, where a single antenna can replace two or more traditional antennas with fixed parameters. For example, some devices are required to operate at multiple frequency bands; however, not at two frequencies simultaneously. This allows to take advantage of reconfigurable antennas, which are capable of switching between the two frequencies without the need of multiple antennas [5].



(a) Omnidirectional Radiation Pattern

(b) Directional Radiation Pattern

Figure 1.2: Omnidirectional vs directional radiation patterns [1].

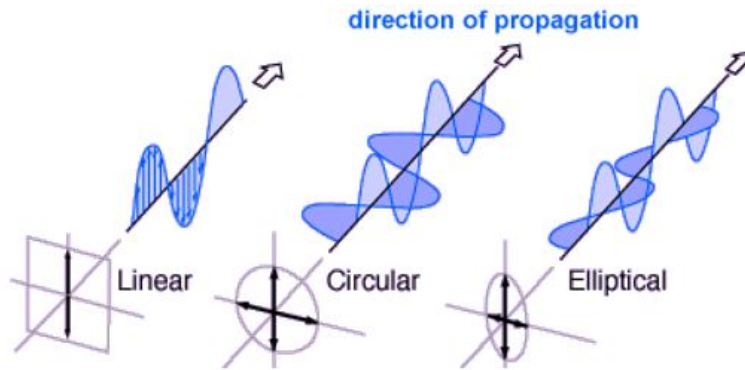


Figure 1.3: Example of polarization patterns [4].

Interestingly, reconfigurability is not limited to switching operating frequencies. In fact, an antenna can also be designed to alter its radiation pattern, polarization, or bandwidth [6]. Figure 1.4 illustrates an example of frequency reconfiguration. The antenna can switch between three states: The first two states represent two different frequencies and the third configuration is a wide-band antenna that encompasses both frequencies [7]. Figure 1.5 is an example of reconfigurable antennas, where the reconfiguration lies in its beam steering capability [8].

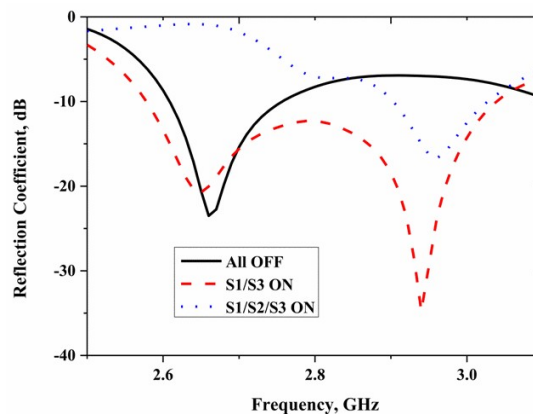


Figure 1.4: Frequency and bandwidth reconfiguration example [7].

In most of the applications, antennas are integrated in devices with limited power supply. Satellites, cellphones, and other electronic devices draw power

from a battery, which emphasizes on the importance of energy consumption of each component. Designing mechanically reconfigurable antennas with minimal power consumption is still a challenging task due to the presence of traditional actuators. Therefore, the main objective of this thesis is to design reconfigurable antennas with new actuation mechanisms to reduce its energy expenditure.

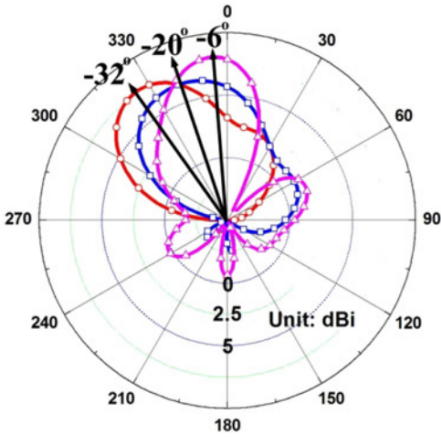


Figure 1.5: Beam steering example[8].

# Chapter 2

## Literature Review

The concept of reconfigurable antennas dates back to the thirties of the last century. In 1934, Friss *et al.*[9] were able to determine the direction of arrival of a wave by steering the nulls of a two-elements array. More recently, researchers around the globe developed new methods to modify the characteristics of an antenna through mechanical reconfiguration. For example, Liu *et al.*[10] were able to shift the operating frequency of their helical antenna by mounting it to a height-adjustable origami structure. Similarly, Tawk [11] changed the frequency of his helical antenna by physically changing the number of turns of the helix. The design relied on hollow helical tubes in which movable arms are able to slide to achieve the required number of turns. Using a soft robot, Blumenschein *et al.*[12] created an inflatable pneumatic structure that carries copper strips placed on top of magnets. Depending on the height of the structure, the magnets ensured that the copper strips were connected to act as a monopole. The soft robot prototype is found in figure 2.1. On the other hand, Nassar *et al.*[13] displaced parasitic patches on top of a slot antenna to change its frequency. Floch and Trad [14] inserted liquid metal between a meander patch and its ground plane.

Zhu *et al.*[15] designed an antenna capable of changing its frequency by rotating a metasurface placed on top of it.

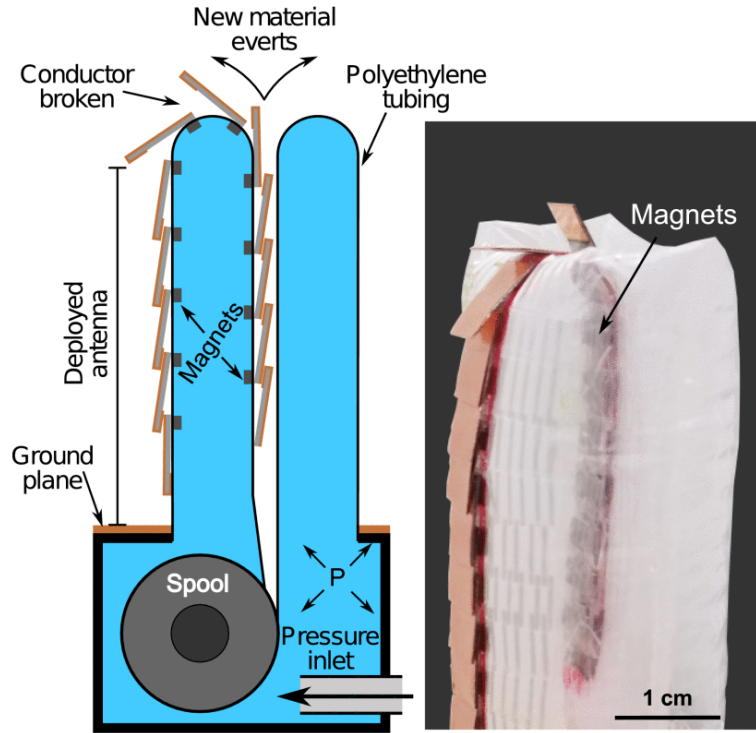


Figure 2.1: A frequency reconfigurable monopole using soft robotics [12].

As for pattern reconfiguration, Zhu *et al.*[8] extended the idea of metasurfaces to achieve beam steering capabilities. Beam steering was also attained in [16], where a liquid metal was used as a director and reflector and was displaced around a Yagi-Uda antenna, as shown in figure 2.2. Mehdipour *et al.*[17] replaced the ground plane of the antenna by a rotating anisotropic carbon fiber plane, where its rotation affects the radiation pattern of the antenna. Boukarkar *et al.*[18] inserted shorting screws between the patch antenna and its ground. By changing the positions of the screws, they were able to control both the frequency and radiation pattern. Concerning polarization reconfigurability, a good example can be illustrated by the work of McMichael [19], where a simple 90 degrees rotation of a truncated corner patch antenna above its fixed L-probe feed allowed for



switching between left-hand circular polarization (LHCP) and right-hand circular polarization (RHCP).

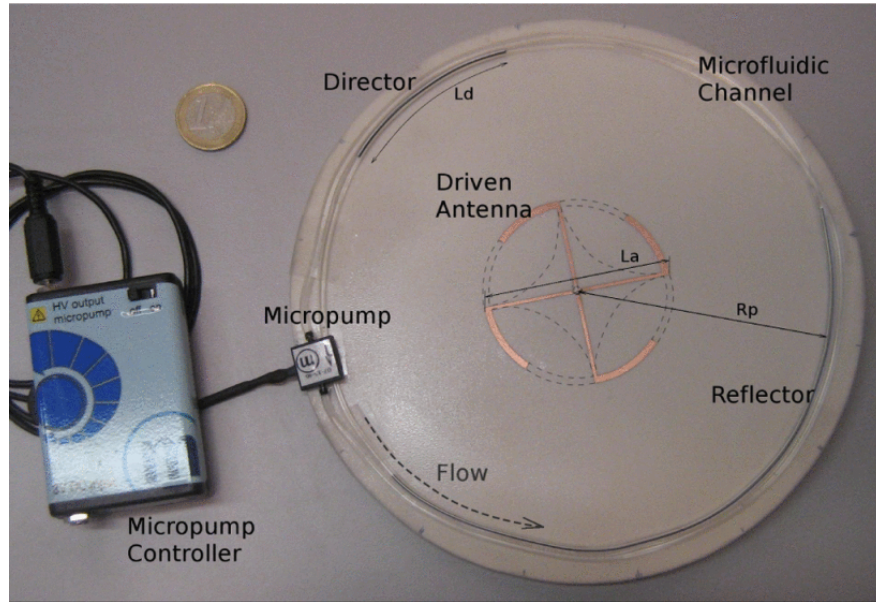


Figure 2.2: Beam steering reconfigurable antenna using liquid metal director and reflector [16].

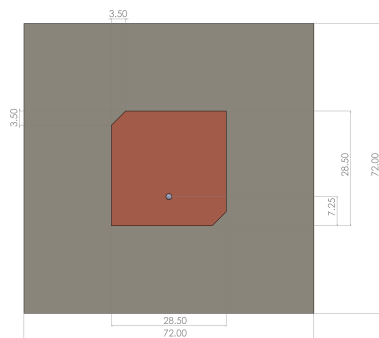
In addition to mechanical reconfiguration, several switching or tuning methods rely on electronic components such as PIN diodes [20],[21], varactors [22],[23],[24], or microelectromechanical (MEMS) switches [25],[26]. Due to their electrical nature, these techniques present many drawbacks despite their fast response. The DC biasing current required for these switches is known to have negative effect on the antenna, leading to a deterioration in its performance[15],[27].

Another important aspect of mechanically reconfigurable antennas is the type of actuators used. Ideally, the actuator should be reliable, provide fast reconfiguration, have low power consumption, and not interfere with antenna's radiation. Mechanical actuators are also widely used in deployable antennas, where their operation is limited to deploying the antenna from a folded state. While the most common type of actuator is a DC motor with all its variations (*e.g.* stepper

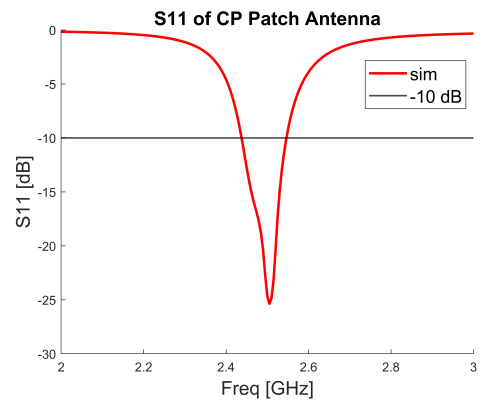
motors, servo motors...) [8],[11],[13],[18],[28] [29], telescopic actuators [10], [30] have been used for linear motion. Furthermore, pumps have been implemented in mechanisms containing liquid metals or other fluids, as seen in [12] and [16]. On the other hand, more recent actuating mechanisms such as shape memory alloys (SMAs) have been introduced in [31] to adjust the height of a helical antenna. Due to their hysteresis and sensitivity to external temperature, special care should be given to the design of the SMA actuators.

In this thesis, we are proposing two reconfigurable antennas based on new and innovative concepts. The first antenna is inspired by the Chladni patterns; whereas the second antenna relies on moire patterns. Each antenna is designed, simulated, and experimentally tested in the anechoic chamber. Moreover, appropriate low power mechanical actuation systems are incorporated in each prototype to ensure automated, yet energy efficient reconfiguration of the proposed antennas.

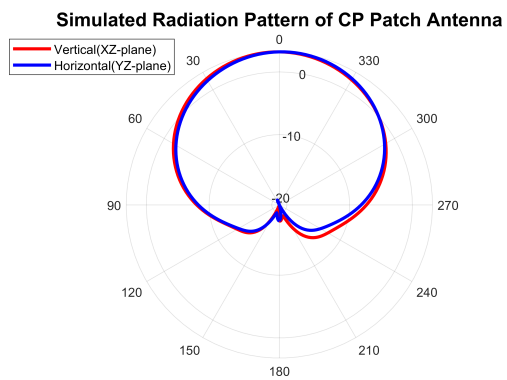
For both designs, we will be using the same patch antenna. The antenna at hand is a truncated edge circularly polarized patch antenna. Its ground plane dimensions are 72x72 mm. The antenna's coaxial feeding offers an advantage over line feeding since the conductive material of the grains could have a reverse effect on the efficiency of the transmission line in the Chladni pattern's antenna. Figure 2.3 shows the detailed dimensions of the patch antenna, along with its S11 bandwidth, its realized gain with a maximum value of 3.2 dB at 0 degrees, and its axial ratio at 2.47 GHZ.



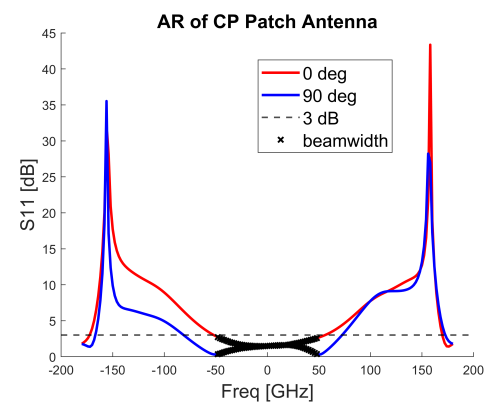
(a) Dimension Drawing



(b) Reflection Coefficient



(c) Total Realized Gain



(d) Axial Ratio

Figure 2.3: CP patch antenna design.

# Chapter 3

## Moiré Patterns Antenna

### 3.1 Background

In the fabric industry, the french term 'moiré' refers to watered silk, characterized by its changing patterns depending on the viewer angle [32]. More generally, moiré patterns are obtained by superposing two layers with similar patterns. The relative displacement between these layers produces new opaque shapes. The two layers are commonly divided into a 'base layer' and a 'revealing layer' [33]. Figure 3.1 shows some examples of the moiré phenomenon with straight and curved lines.

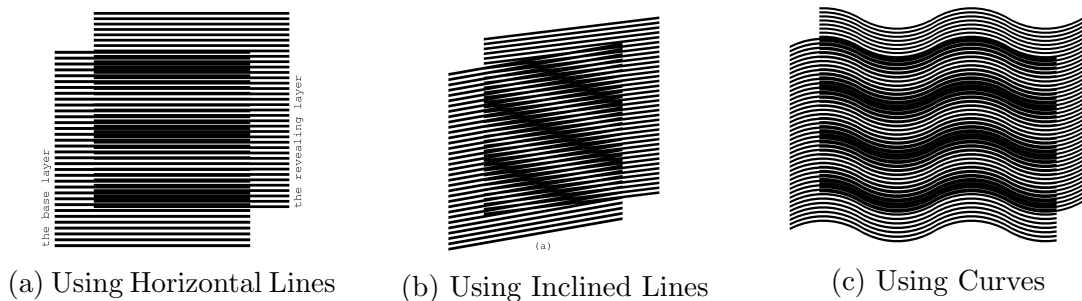


Figure 3.1: Typical examples of moiré stacking [33].

Due to its high sensitivity to displacements, the moiré effect was beneficial for many applications. For example, in [34], the moiré phenomenon was used to analyse strain. When the object with moiré fringes is strained and deformed, it can be compared to a reference layer. The resulting moiré pattern is used to determine the direction and amplitude of the strain. On the other hand, Cadarso *et al.*[35] created high-resolution patterns that can be used in document counterfeiting. Figure 3.2 shows how the base layer looks like on the document; however, when it is superimposed with a revealing layer, meaningful words appear, which confirms the authenticity of the document.

For our antenna application, two copper layers with horizontal line patterns are superimposed and rotated with respect to each other on top of an antenna. The produced moiré effect changes the density of the 'grid' created by the two layers of copper, which affects the RF emissions of the antenna. This allows us to reconfigure the radiation pattern depending on the rotation angle.

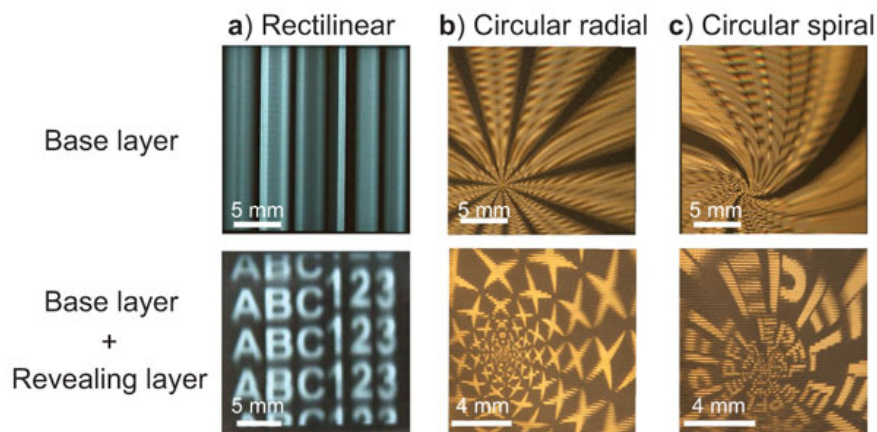


Figure 3.2: Moiré pattern in document counterfeit [35].

## 3.2 Working Principle

As previously mentioned, the mechanical reconfiguration is possible through placing two circular patches, each consisting of a substrate and a copper layer, above a patch antenna. Figure 3.3 shows the main components of the reconfigurable antenna. The two identical moiré patches are placed such as their copper layers are in direct contact. The separation distance between the copper layer and the driven antenna is optimized to 10 mm using ANSYS HFSS 2020 R1. The driven antenna is a circularly polarized, truncated edge, patch antenna. In 3.4, rotating one moiré patch with respect to the second fixed patch creates a new grid shape, resulting in almost vertical lines that are perpendicular to the original horizontal stripes. As we increase the rotation angle, the grid density increases, and the number of appearing vertical lines increases.

Although the rotation angles are of small increments, the major change in the resulting shape due to the moiré phenomenon has a very interesting effect on the antenna's radiation pattern. The surface current distributions presented in figure 3.3 gives us a clearer explanation on the polarization reconfiguration from linear vertical polarization at 0 deg rotation, to linear horizontal polarization at 10 deg, and to circular polarization at 30 deg. In figure 3.3(a), the maximum surface current on the moiré patches is in the proximity of the radiating edges of the base antenna. These horizontal currents act as a reflector to most of the horizontal components of the traveling wave, hence resulting in a vertically polarized antenna. At 10 deg, figure 3.3(b) indicates the existence of a similar situation; however, in this case the current is maximal along the newly appearing vertical lines of the moiré effect. The location of these vertical lines, near the edges of the antenna along its width, reflect most of the vertical components

of the traveling wave, leading to a horizontally polarized antenna. At larger rotation angles, in particular at 30 deg, the high grid density allows for an even surface current throughout the copper layer, as seen in figure 3.3(c). This allows the travelling wave to have the same polarization as the driven antenna, a left-handed circular polarization. More interestingly, although the polarization is still the same, the moiré patches focus the beam and increase its directivity and gain, which is discussed in a later section.

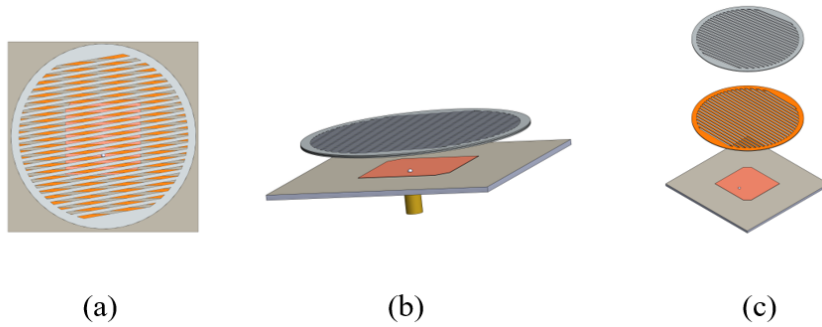


Figure 3.3: Simplified illustrations of the working principle of the proposed antenna seen as (a) a top view, (b) a perspective view, and (c) an exploded view.

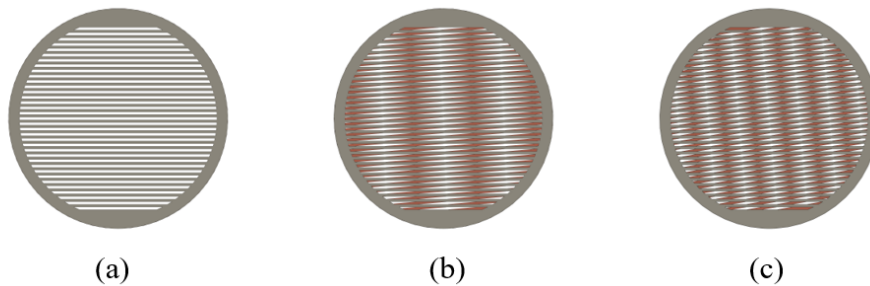


Figure 3.4: Moiré patterns obtained by rotating two circular patches with a copper layer by (a) 0 deg, (b) 10 deg, and (c) 30 deg.

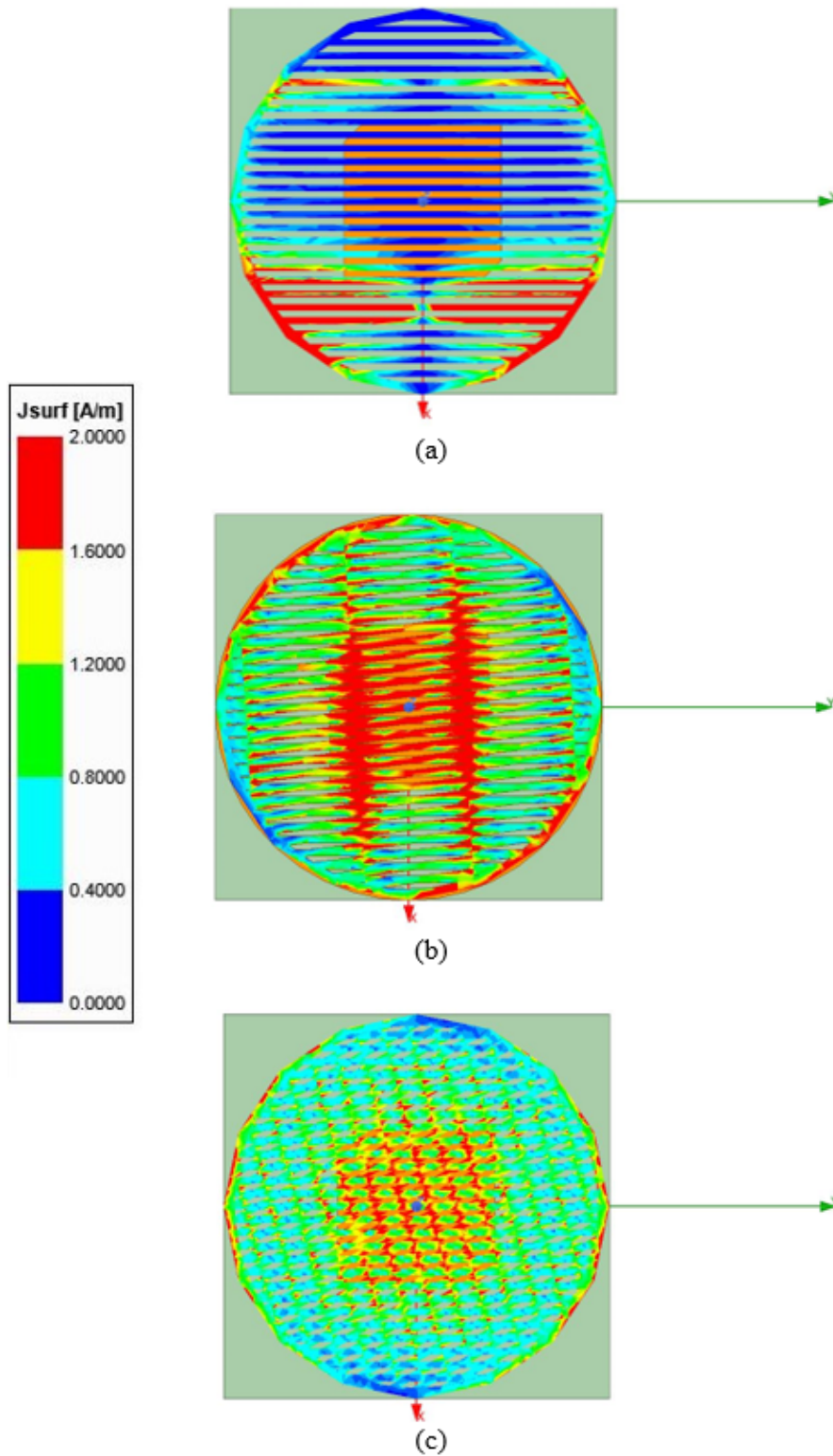


Figure 3.5: Simulated surface current distribution on the moiré patches at (a) 0 deg rotation, (b) 10 deg rotation, and (c) 30 deg rotation.



### 3.3 Mechanical Design

In this design, the moiré effect is obtained by rotating two circular patches with horizontal lines patterns. The patches are rotated using a ratchet mechanism with two shape memory alloy (SMA) actuators. A prototype design is presented in figure 3.6, along with its cross-sectional and exploded views.

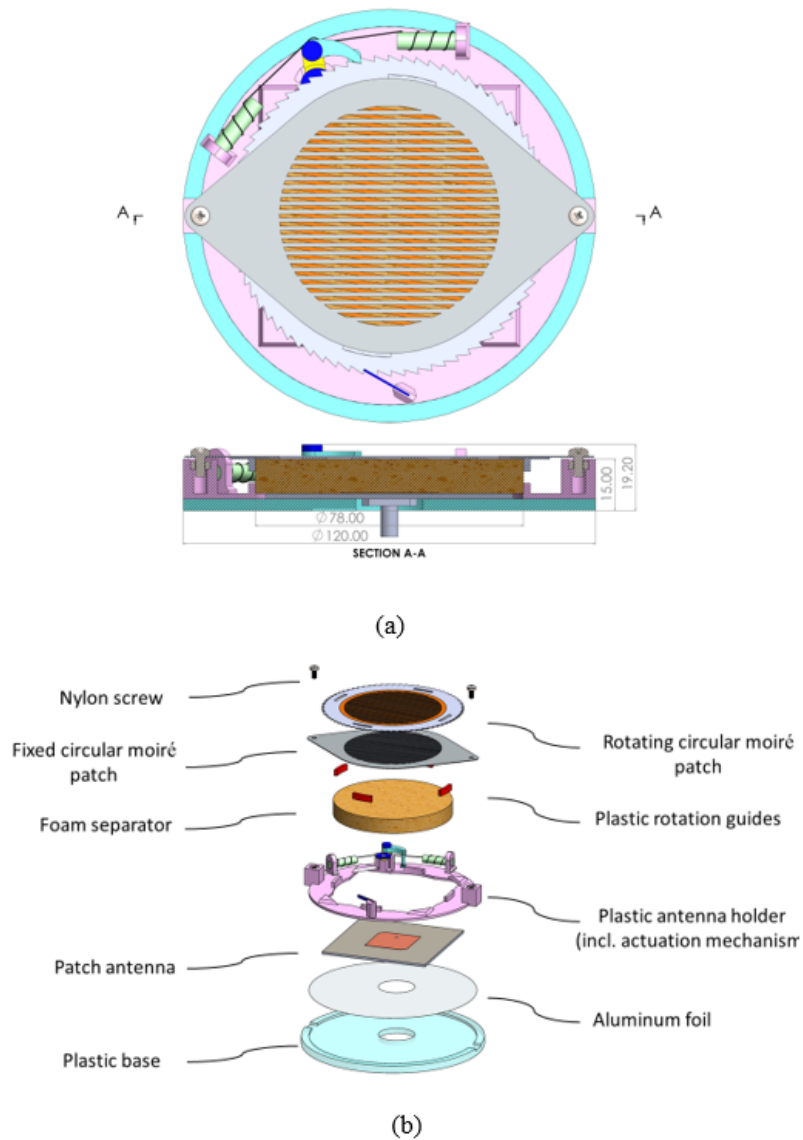


Figure 3.6: CAD representation of the proposed reconfigurable antenna seen as (a) a top view along its cross-sectional view, (b) an exploded view.

The listed components below are briefly described in the next subsections:

- Truncated edges patch antenna.
- Moiré circular patches.
- Ratchet mechanism.
- SMA actuator.
- Supporting structure.

### 3.3.1 Moiré Circular Patches

Each moiré patch is made of 0.4 mm FR4 substrate that is copper cladded on one side only, as shown in figure 3.7 . Within a circle of 64 mm diameter from the center of each patch, horizontal stripes of 1.2 mm width and 1.2 mm separation distance are milled using a mechanical CNC machine. The width and separation distance of the horizontal stripes on the moiré patches are chosen to be around one hundredth of the driven antenna's wavelength.

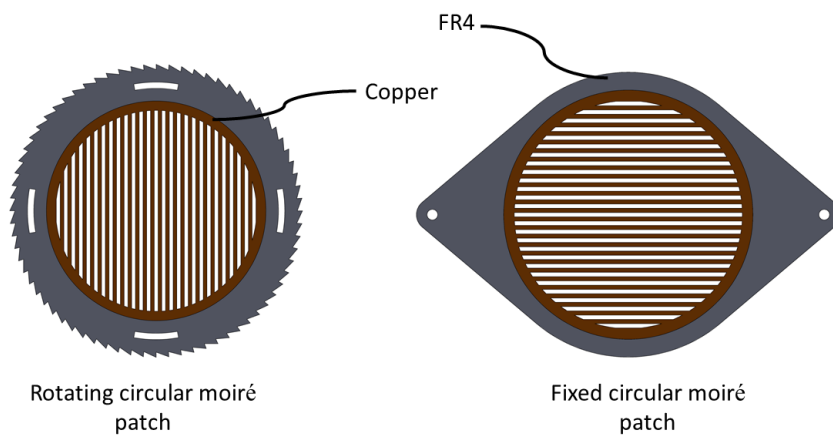


Figure 3.7: Moiré patches made from one sided copper FR4 substrate.

The outer shape of the fixed top patch is laser cut and fixed to the supporting structure via two M3 screws. The rotating patch has outer teeth laser cut on its boundary which will be used for the ratcheting mechanism. The ratchet teeth are designed to allow 5 degrees rotation increments over the full 360 range. Once the two patches are superimposed with the copper layers touching each other, any rotation angle will produce a moiré effect. Some examples of the effect of rotating the two patches is shown in figure 3.8.

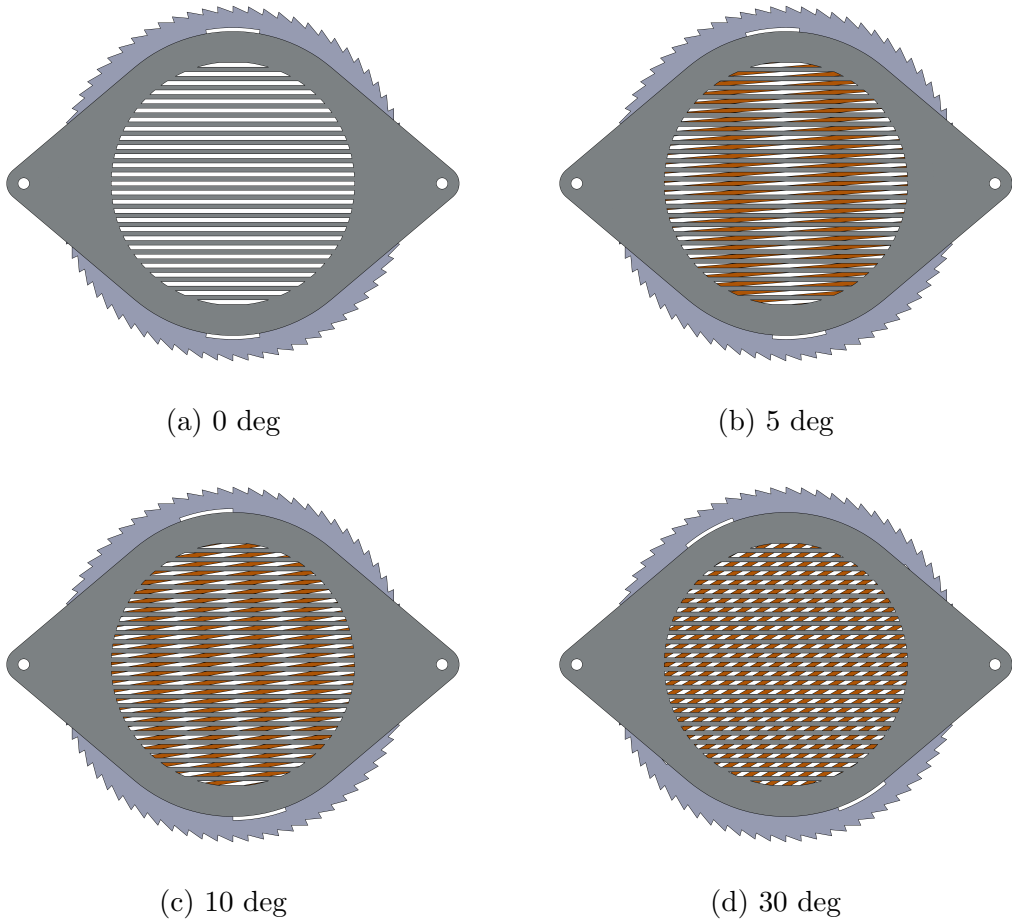


Figure 3.8: Moiré effect by rotating the teethered disc.

### 3.3.2 SMA Actuator

Shape memory alloys (SMA) are materials that exhibit shape memory and pseudoelastic effects. These interesting phenomena allow designers to use SMA wires as actuators. Using the shape memory effect, SMA wires can be trained to different shapes such as springs that return to their initial shapes upon heating above a transition temperature. On the other hand, a straight SMA wire can also be used as an actuator by relying on the pseudoelastic effects, where the wire can be effectively contracted by more than 3% of its original length when heated [36]. While an SMA wire actuator produces more forces, a spring shaped SMA enable a larger stroke with smaller forces. Their low weight, along with their high energy density and shape versatility, renders them a suitable competitor for the more traditional actuators such as DC [37]. SMA actuators have many applications in the robotic, biomedical, and aerospace industries [38]. They are also typically used in the space antennas field for deployable structures [39], or for repositioning a reconfigurable helical antenna [31].

The typical disadvantages of SMAs, such as their high temperature requirements and non-precise positioning due to their hysteresis loop [40] are overcome by properly designing the proposed ratchet mechanism, discussed in the subsequent subsection. For the proposed design, a 0.02" (0.508 mm) shape-memory Nitinol (Nickel-Titanium alloy) wire is used. The helical spring shape of the SMA is obtained by winding the wire around a 6 mm screw and firmly fixing both ends using two nuts. The setup is then heating in an oven at 500 °C for 50 minutes to train the wire. The final step is to quench the wire in cool water. The previously straight wire has a now a new helical shape. After deforming the spring shape, the application of heat above the wire transition temperature, typically using an electric current, makes the spring return to its initial shape.

### 3.3.3 Ratchet Mechanism

The proposed actuation system, represented by the ratchet mechanism and two SMA actuators, is shown in figure 3.9 and figure 3.10. A conventional ratchet mechanism typically consists of two pawls and at least two metallic springs. In the proposed mechanism, a rubber band replaces the first metallic spring, whereas a compliant plastic rod, shown as rectangular blue rod in figure 3.9(a), replaces the second pawl and its spring. The design tends to minimize the presence of metallic parts in the antenna's system.

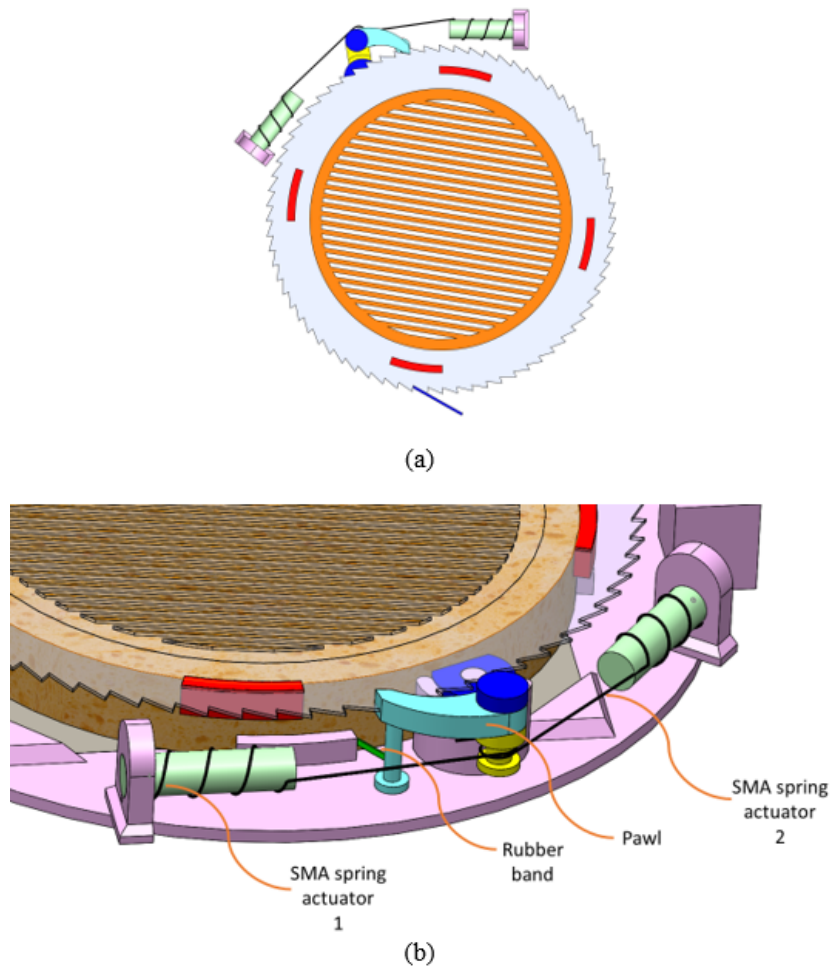


Figure 3.9: CAD representation of the proposed actuation mechanism as (a) a top view, (b) an annotated perspective view.



Figure 3.10: Actuation mechanism used in the prototype.

In figure 3.11, the pawl is in contact with the teathed disc and is attached to the two SMA helical springs. When an electric current is applied through SMA spring actuator 1, the spring contracts by less than 10 mm, moving the pawl and the teathed disc by 5 degrees. The precise 5 deg rotation is guaranteed by mechanical stops, which do not allow the pawl to travel further distances. At this stage, the applied voltage on SMA spring 1 is disconnected, and SMA spring 2 is activated. The pawl travels back by 5 deg and is now placed in contact with a different tooth, ready for the next rotation. The role of the compliant rod is to allow rotation in one direction only, i.e., only in the direction in actuator 1. When SMA actuator 2 is activated, the compliant rod's job is to hold the teathed disc in its place, preventing it from travelling back with the pawl. Throughout the movement of the pawl, the rubber band exerts a small inward force toward the center of the teathed disc to keep the pawl in contact with the teeth at all times. The mechanical stops are used to increase the precision of the mechanism, by bypassing the hysteresis behavior of Nitinol and the deployment of feedback control loops. Since the components of the actuation system are in contact with the SMA wires that heat up, they need to have high temperature resistance properties. PLA has low heat resistance; therefore, these components are 3D

printed with “High Temp Resin V1” from Formlabs. This material has the ability to resist temperature up to around 280 °C before deforming.

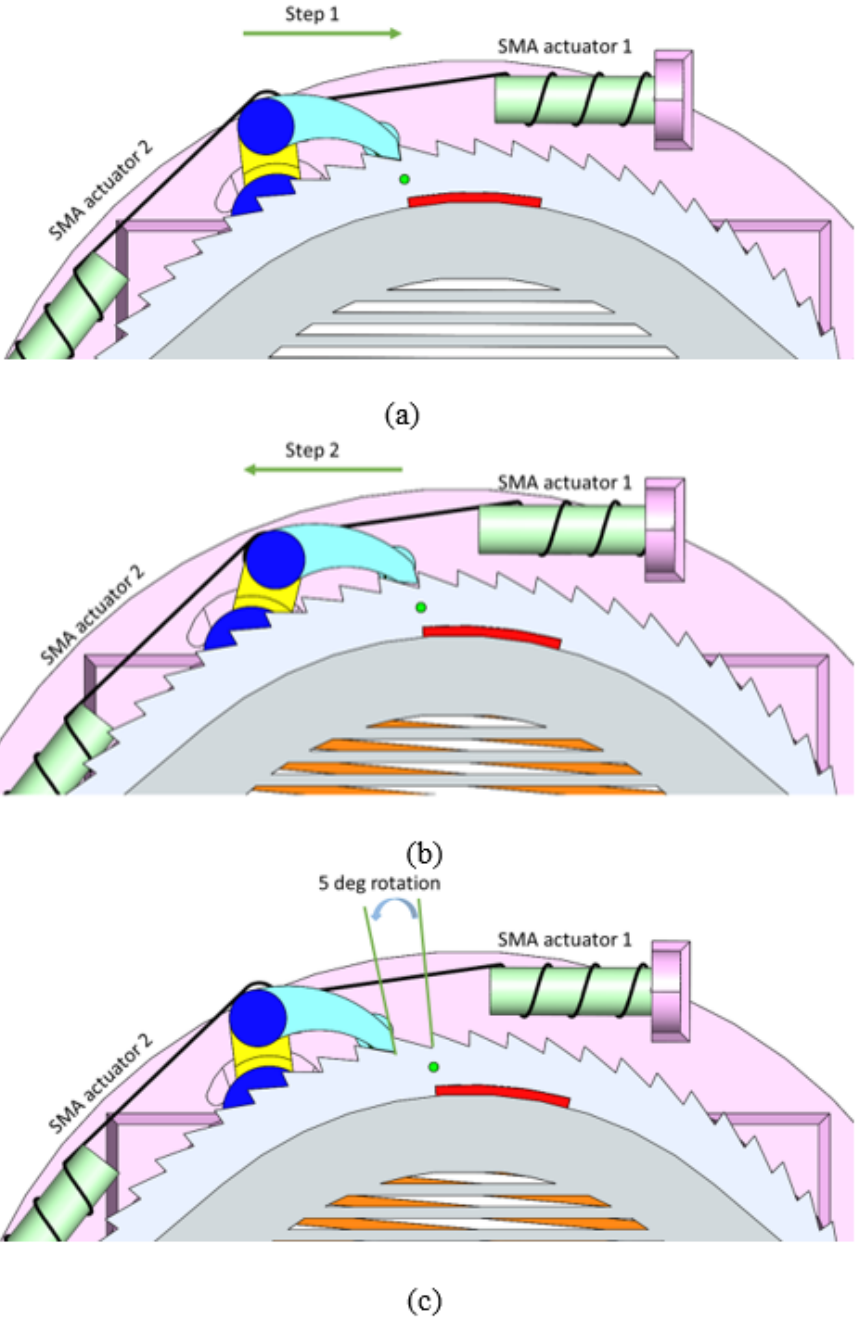


Figure 3.11: CAD representation of the proposed actuation mechanism as (a) a top view, (b) an annotated perspective view.

The presented actuation mechanism is characterized by its speed, its precision, and low energy consumption. The total required energy is low due to lightweight rotating structure, and the short time needed for contracting the SMA spring (less than one second). The other advantage of this system is the absence of metallic and magnetic parts and housings usually used in traditional motors. Finally, the mechanism is very flexible in terms of the occupied volume and space. The SMA wires can be placed at different places in the structure depending on the design constraints. Moreover, the shape of the SMA actuator can also be modified, for example two straight wire (pseudoelastic effect) or a flat spring (S-shaped).

### 3.3.4 Previous Designs

The final design of figure 3.6 is the result of multiple previous designs and prototypes, which were all optimized and re-designed accordingly. Figure 3.12 shows some of the previous fabricated prototypes.

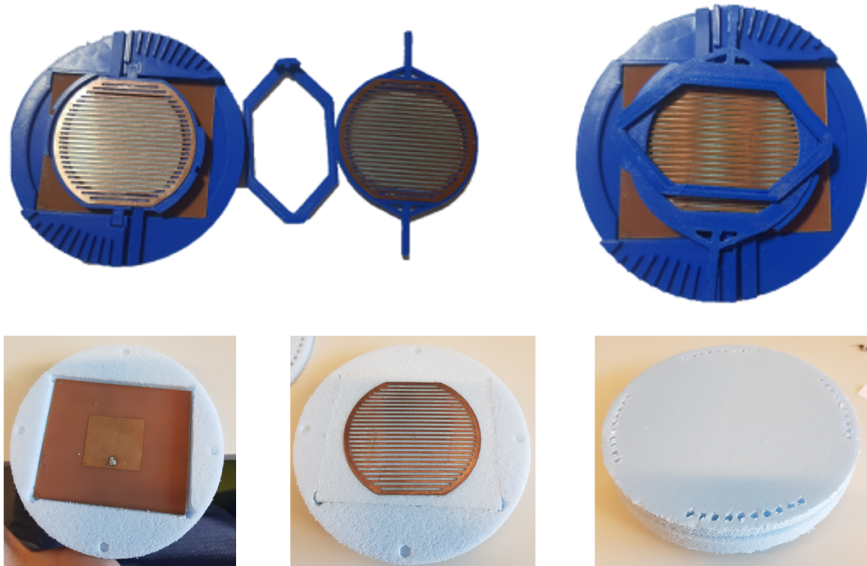


Figure 3.12: Previous fabricated prototypes.



### 3.4 Simulations and Experimental Results

All the simulations and experimental work presented in this section are based on the prototype presented in figure 3.13. The blue Styrofoam in the background is designed to hold and fix the antenna setup in the anechoic chamber during the measurement.

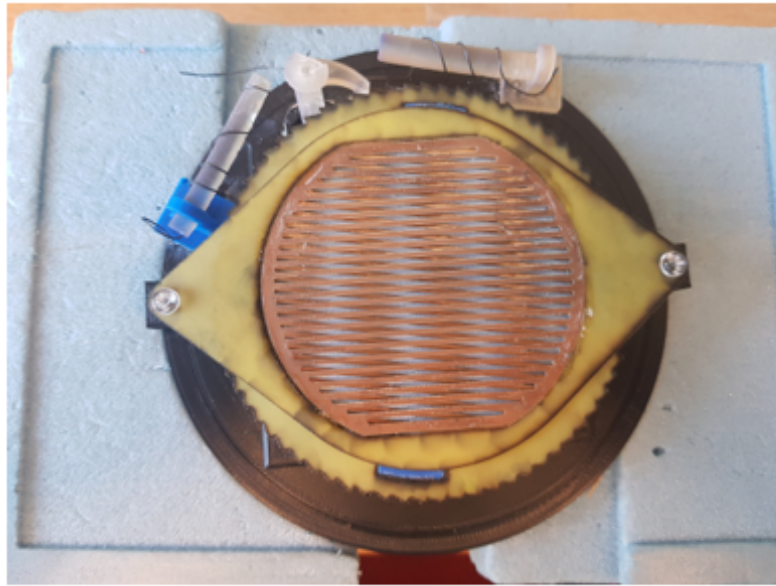


Figure 3.13: Fabricated antenna prototype.

Figure 3.14 shows a slight tuning in the S11 bandwidth from 2.47-2.52 GHz at 0 deg rotation (the moiré patches having identical orientations), to 2.53-2.63 GHz at the other states, in particular at the chosen rotation angles of 10 deg and 30 deg.

As for the radiation patterns, figure 3.15 depicts the vertical (gain Theta) and horizontal (gain Phi) components of the radiated beam. The effect of the moiré phenomenon, discussed earlier using the surface current distributions, is more apparent in these plots. At 0 deg and 10 deg, figure 3.15(a) and figure 3.15(b) show a different dominant co-polarization component with a cross-

polarization isolation of around 10 dB, suggesting that the co-polarization signal can be received with minor noise. Figure 3.15(c) indicates that at 30 deg, the peak gain of both components is of similar magnitude, implying a circularly polarized wave. The resulting beam is LHCP, having the same handedness as the driven antenna.

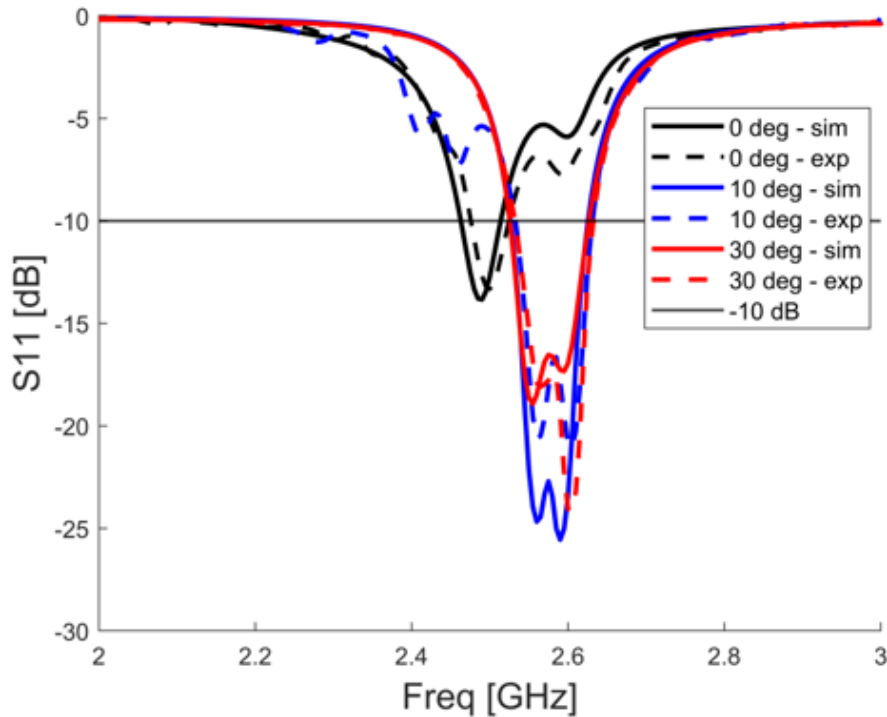


Figure 3.14: Simulated and measured S11 of the proposed antenna.

figure 3.16 reveals the good matching between the simulated and experimental radiation patterns of the dominant components. The dominant components are namely the vertical component at 0 deg, the horizontal component at 10 deg, and both at 30 deg due to the circular polarization of the antenna at this state. figure 3.17 shows the total realized gain at the three states. It can be observed that the beam becomes more directed as the rotation angle increases. The 3 dB beamwidth of the total realized gain decreases from 100 deg at 0 deg

rotation angle, to 52 deg and 48 deg at the second and third states, respectively. As for the peak realized gain, it increases from around 3 dB at the first state, up to more than 5 dB at 30 deg rotation angle.

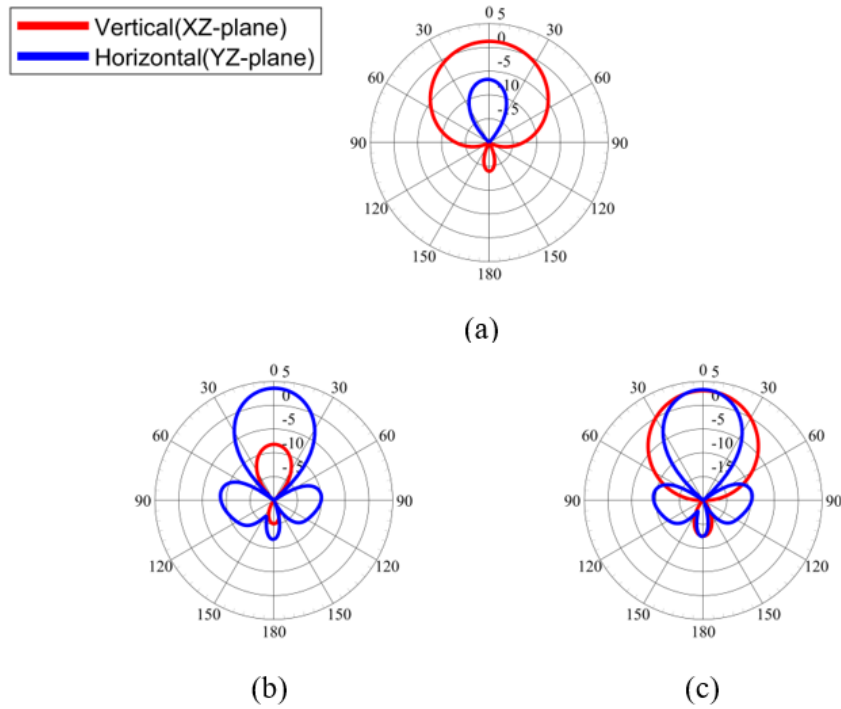


Figure 3.15: Simulated radiation patterns at (a) 0 deg rotation, (b) 10 deg rotation, and (c) 30 deg rotation.

Figure 3.18(a) and figure 3.18(b) show the axial ratio of the reconfigurable antenna in its circularly polarized state (30 deg rotation angle). Although the axial ratio is not less than 3dB throughout the antenna's impedance matching bandwidth, the antenna still exhibits a circular polarization behavior over 20 MHz of the bandwidth. Interestingly, the axial ratio performance of the reconfigurable antenna is similar to that of the driven antenna, shown in figure 3.18(a). As seen in figure 3.18(b), the radiated beam displays circular polarization throughout its beamwidth of 48 deg (-24 deg to +24 deg).

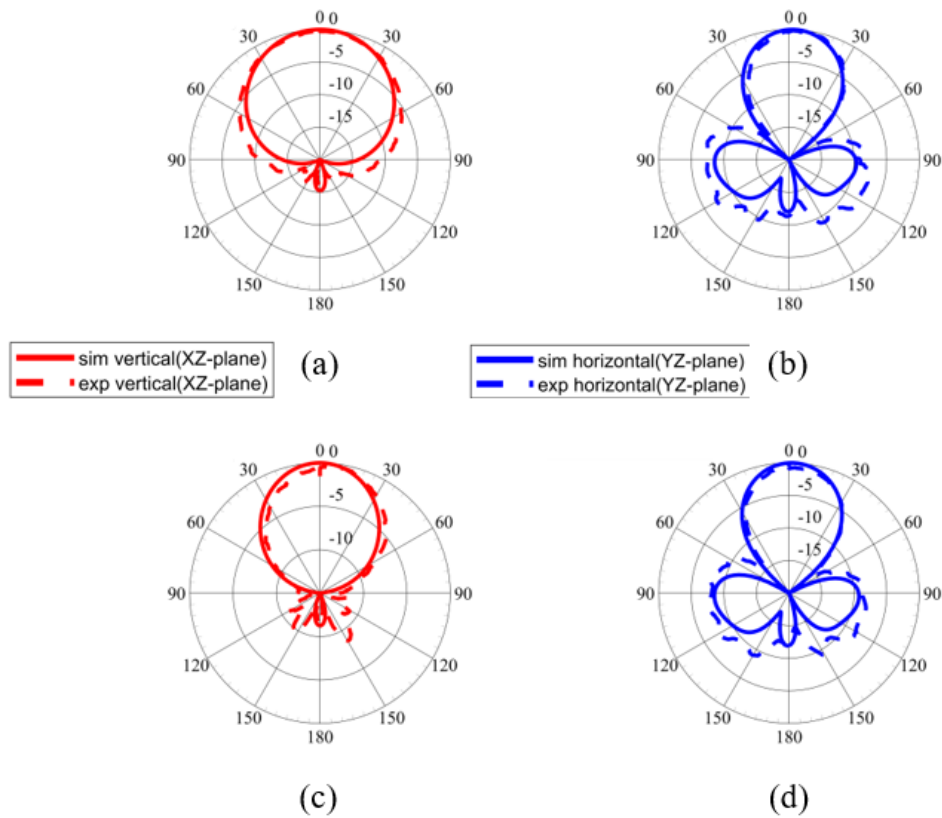


Figure 3.16: Normalized simulated and measured radiation patterns of the dominant components at (a) 0 deg rotation, (b) 10 deg rotation, and (c)(d) 30 deg rotation.

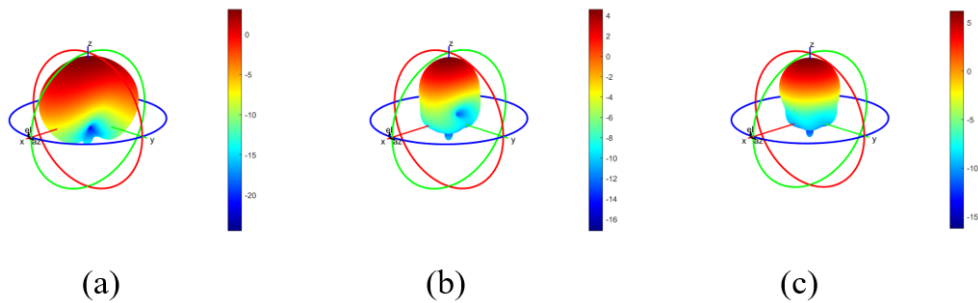


Figure 3.17: Three-dimensional realized gain patterns at (a) 0 deg, (b) 10 deg, and (c) 30 deg rotations, respectively.

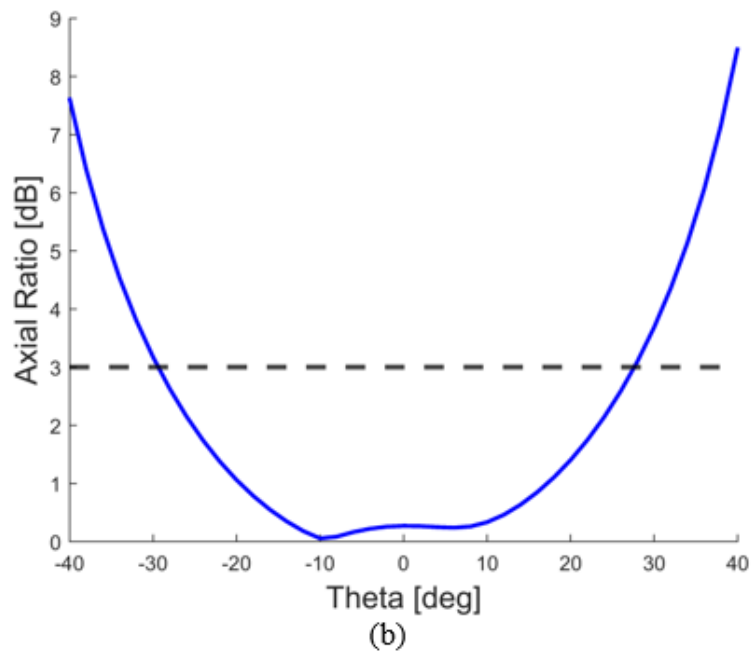
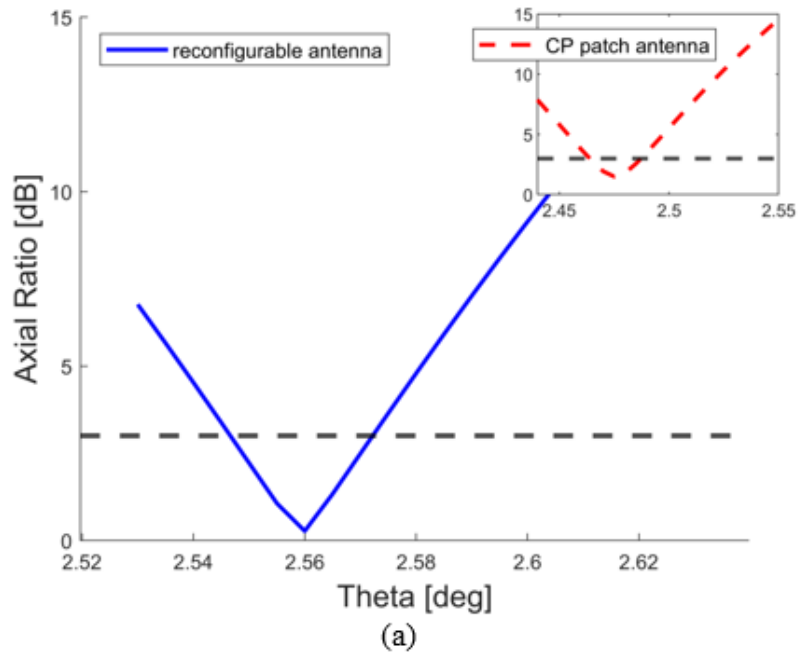


Figure 3.18: Axial ratio of the proposed antenna at 30 deg (a) throughout its S11 bandwidth, and (b) at 2.56 GHz.

# Chapter 4

## Chladni Patterns Antenna

### 4.1 Background

From unnoticeable particle-scale oscillations to devastating earthquakes, vibrations are a fundamental concept in the physics of the world we live in. In engineering applications, designers take special care of vibrations in certain applications that operate at high speeds and temperatures, such as engines, turbines, or other heavy machinery [41]. On the other hand, vibrations are highly desirable in other fields, especially in acoustics. In fact, whether to be emitted or received, all sounds rely on vibration [42].

When a membrane or thin plate vibrates, it creates a mode shape depending on the associated eigenfrequency and eigenmode [43]. In 1787, Ernst Chladni was able to visualize these eigenmodes by sprinkling sand on top of a vibrating plate. Due to the vibrations, the sand particles travel to the nodal lines (zero displacement lines), creating fascinating patterns as seen in figure 4.1 [44]. These patterns are highly sensitive to the material properties, plate shape, external loads, and boundary conditions [45]. Figure 4.2 shows some of the ex-

perimental patterns obtained using the copper filings. It should be noted that the power input needed to create the shapes was proportional to the increase in frequency.

For this antenna idea, we intend to benefit from Chladni patterns by manipulating conductive grains. By relying on vibrating actuators, the different obtained shapes are placed on a substrate on top of an antenna. Each shape constitutes a state of the reconfigurable antenna. The main advantages of such antenna are the possibility of having a large number of states (shapes) using one or very few actuators.

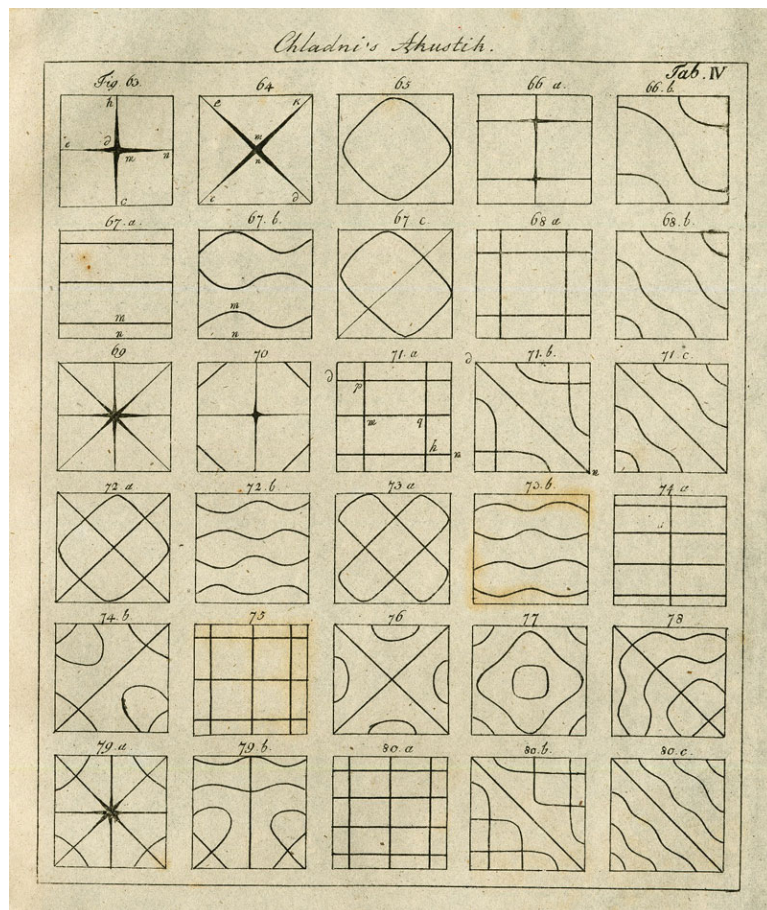


Figure 4.1: Patterns obtained by Ernst Chladni in 1787 [44].

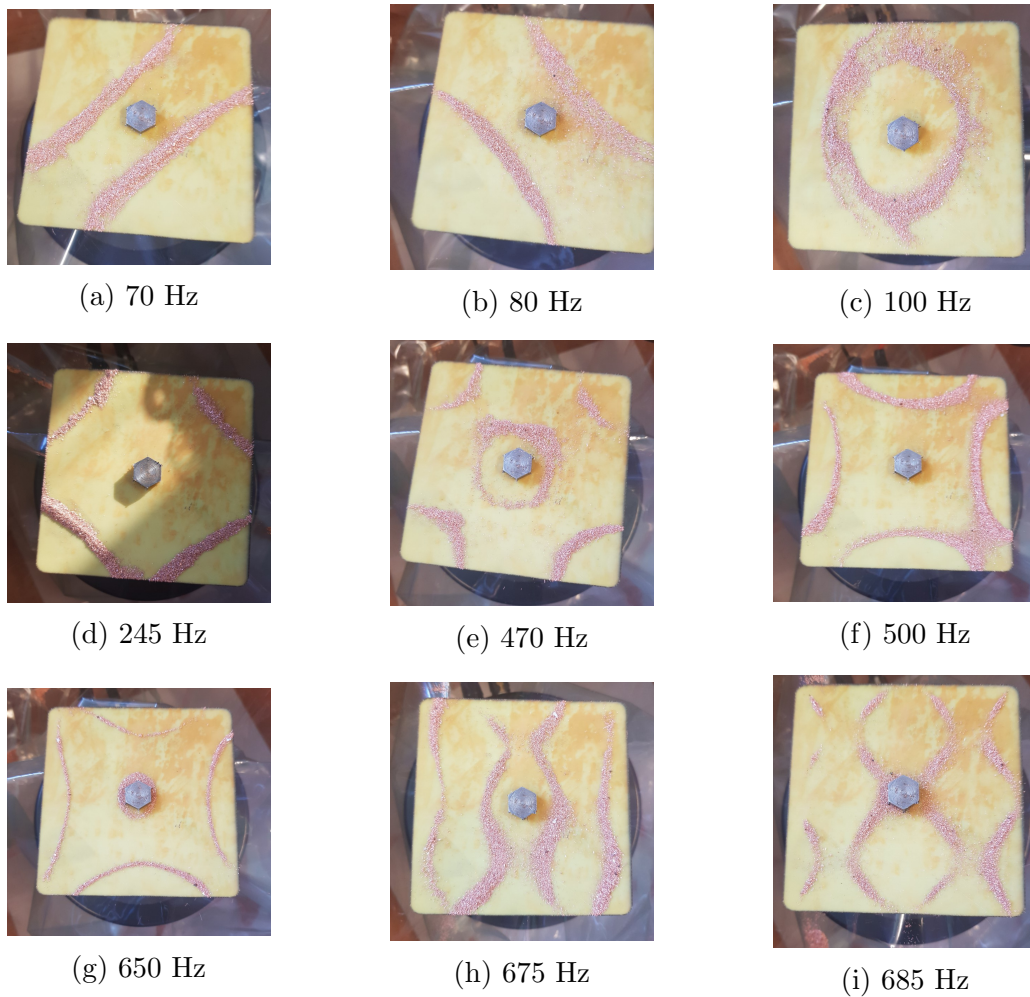


Figure 4.2: Chladni patterns obtained using copper filings.

## 4.2 Mechanical Design

Despite the fact that the design of this antenna is not finalized, it has to rely on the following essential components:

- Patch antenna.
- FR4 substrate.
- Conductive grains.
- Vibrating actuators.



- Mechanism to preserve the obtained patterns.
- Additional Components.

Figure 4.3 presents an exploded view of most of the components of the proposed antenna. Next, a brief description of each element is introduced.

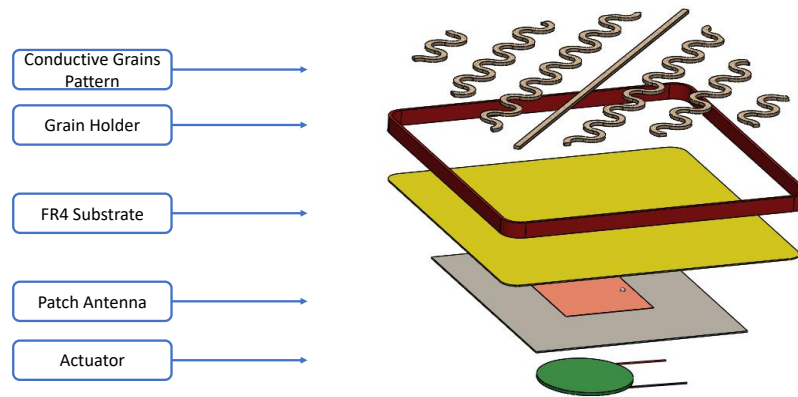


Figure 4.3: Main components of the Chladni patterns antenna.

#### 4.2.1 FR4 Substrate

This substrate serves as a thin plate for the vibration of the grains. However, since it is placed on top of the patch antenna, we eliminated all the metal choices. After some experiments with different Plexiglas plates (2mm, 3mm, and 5mm thickness) and different thickness of FR4 substrates (0.1 mm, 0.4 mm, and 1.5 mm thickness), the most suitable choice was a 100x100x0.4 mm FR4 square plate with filleted edges. The selection criteria was the plate's ability to support the vibrating gain and to vibrate with enough displacement to cause visible Chladni patterns.

## 4.2.2 Conductive Grains

A good candidate to replace sand particles with conductive materials was copper powder. The first iteration of the process was to produce copper filings by grinding a copper bar. The resulting grains were inconsistent in size and shape and contained many defects. During the experimental work, these grains created the desired patterns, but with no sign of electric conductivity. After consulting the literature, [46], [47], and [48] indicated that there exists a minimal pressure for the copper powder to be conductive. And even at higher pressures, the conductivity of the powder is several orders of magnitude lower than that of metal copper. This low conductivity is due to several causes, such as the shape of the grains that affect the surface contact area, the properties of the non-conductive oxide layer on the grains, in addition to the applied pressure.

An alternative to copper powder was aluminum foil. Even when cut to millimeter size pieces, the foil exhibited excellent conductivity measurement. The only challenge using this material is that obtaining small and consistent pieces is difficult, especially that it is impossible to laser cut on the common laser cutting machines. To test the effect of the shape and size of the pieces on vibration, we laser cut different shapes and dimensions into plastic sheets and did a vibration test for each. The included shapes were of circular, triangular, square, hexagonal, and star profiles. The size of each shape varied from 2 mm to 5mm. The results were bench marked against the shape obtained from the copper filings.

Figure 4.4 reveals the some of the tested shapes. On the other hand, figure 4.5 shows the benchmark copper powder pattern. The tests showed that the square and triangular shapes made the best shapes, whereas the star and hexagonal profiles were the worst. In the end, the square profile was chosen since

it is easier to obtain and provides better overlap than triangles. The next test was to see if the plastic sheets results would be similar to the shapes obtained using aluminum foils. Therefore, squared aluminum foil pieces were manually cut and subjected to the same vibrating conditions. The results indicated a good matching between the two, as seen in figure 4.6.



(a) Stars 5mm



(b) Circle 5mm



(c) Triangle 5mm



(d) Square 5mm



(e) Hexagon 5mm



(f) Hexagon 3mm

Figure 4.4: Shape and size comparison of plastic sheets.



Figure 4.5: Copper powder shape benchmark.



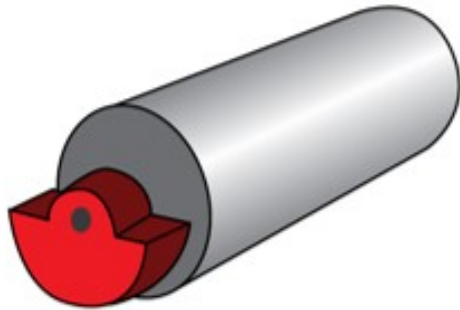
(a) Using Plastic Sheets



(b) Using Aluminum Foil

Figure 4.6: Comparing the results of the patterns using plastic sheets Vs Aluminum foil.

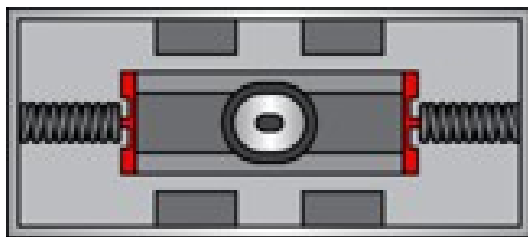
### 4.2.3 Actuators



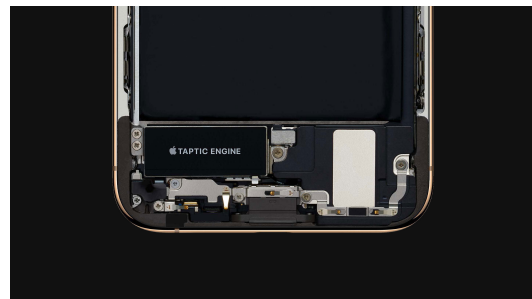
(a) ERM [49]



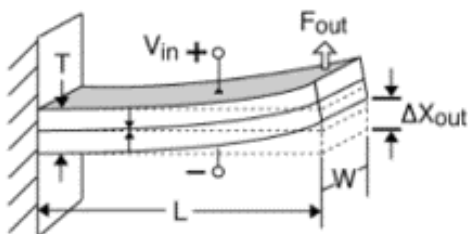
(b) ERM in PS4 Controller [50]



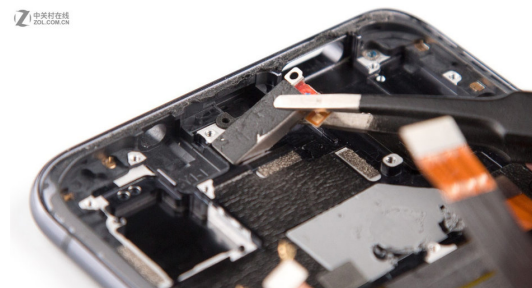
(c) LRA [49]



(d) Taptic Engine (LRA) in iPhone [51]



(e) Piezo [52]



(f) SoundCasting actuator (Piezo) in Vivo NEX [53]

Figure 4.7: Types of haptic actuators with relevant applications.

Commonly found in today's phones and gaming controllers, haptic actuators deliver mechanical feedback through vibrations. These actuators are usually small and have low power consumption, which make them ideal for our antenna. However, there exist three types of actuators, each with different characteristics: Eccentric Rotating Mass (ERM), Linear Resonant Actuator (LRA) and Piezo

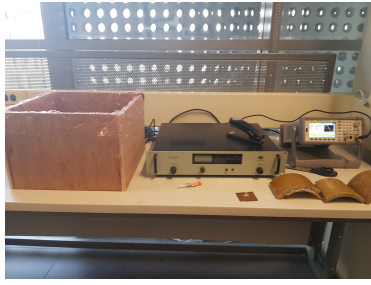
actuators [49]. A graphical representation of each type of actuator, along with a real world application, is presented in figure 4.7.

As its name indicates, eccentric rotating mass motors rely on the rotation of an unbalanced mass. Although cost effective, these actuators are slow, have high energy consumption, produce motion across two axes and their amplitude and frequency are coupled. On the other hand, linear resonant actuators move a mass across one axis using a magnetic coil. LRA's are more efficiency than ERM's; however, they operate over a narrow frequency range. As for piezo actuators, they overcome most of the disadvantages of the previous two actuators: they are fast, have wide frequency bandwidth, and are electrically efficient. The only downsides are they higher cost and the need for drivers to deliver the high voltage needed for their proper operation. For this antenna, we intend to use LRA or Piezo actuators depending on the analysis of the shapes needed and the number of actuators. As for the power consumption of both actuators, it is estimated to be in the 100's of milliwatts or even less for each actuator.

### **4.3 Simulations and Experimental Results**

After choosing the best material and dimensions for the substrate to be vibrated, the following setup was adopted to create Chladni patterns using the copper filings (see figure 4.8):

- Brüel & Kjær Vibration Exciter - Type 4809.
- Brüel & Kjær Power Amplifier Type 2718.
- Wave Generator.
- 100x100x0.4 mm FR4 plate.
- Wooden box and nylon covers.



(a) Wave Generator and Power Amplifier



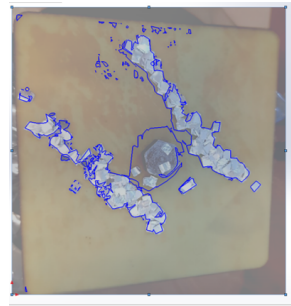
(b) Vibration Exciter with Protective Nylon Covers

Figure 4.8: Vibration setup.

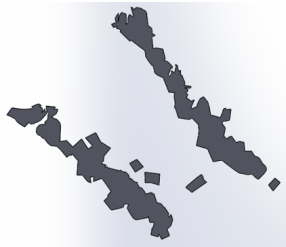
To further prove the reconfiguration concept of this antenna, a sample simulation was reproduced. As a first step, the image contained the Chladni Pattern is processed on SolidWorks using the Auto-trace feature. The 2D shape obtained from the aluminum foil is then transformed to a 3D body to be imported to the simulation on HFSS. Figure 4.9 visualizes the steps of this process.



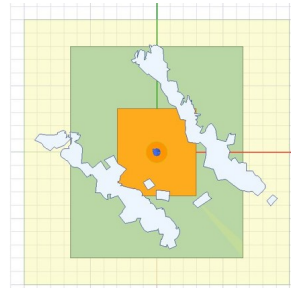
(a) Experimental Result



(b) Auto-Trace on SolidWorks



(c) Edited and cleaned Auto-Trace on SolidWorks



(d) Simulated Antenna On HFSS

Figure 4.9: Steps to simulate experimental Chladni patterns

The results of this simulation are compared to the antenna with the FR4 substrate only (without the foil). Figure 4.10 shows a frequency tuning from 2.345 GHz to 2.32 GHz; whereas figure 4.11 shows same similar radiation patterns for both states.

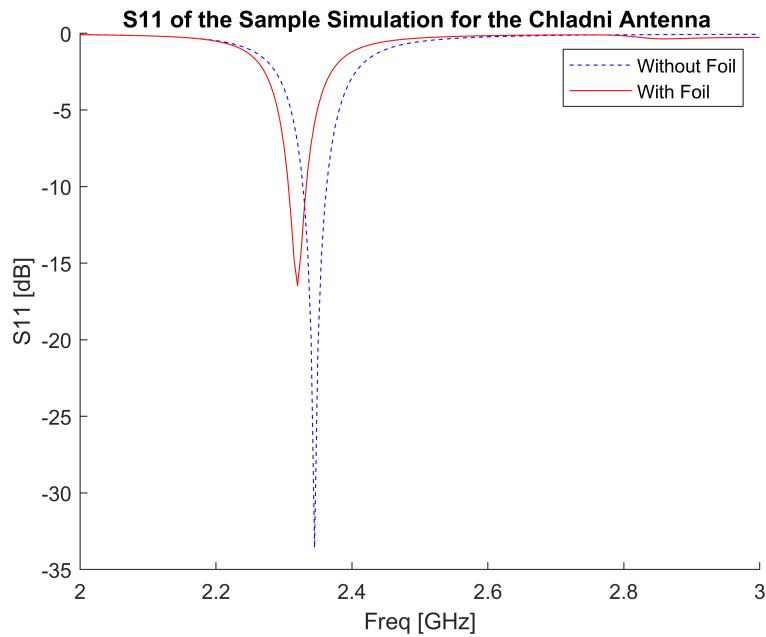
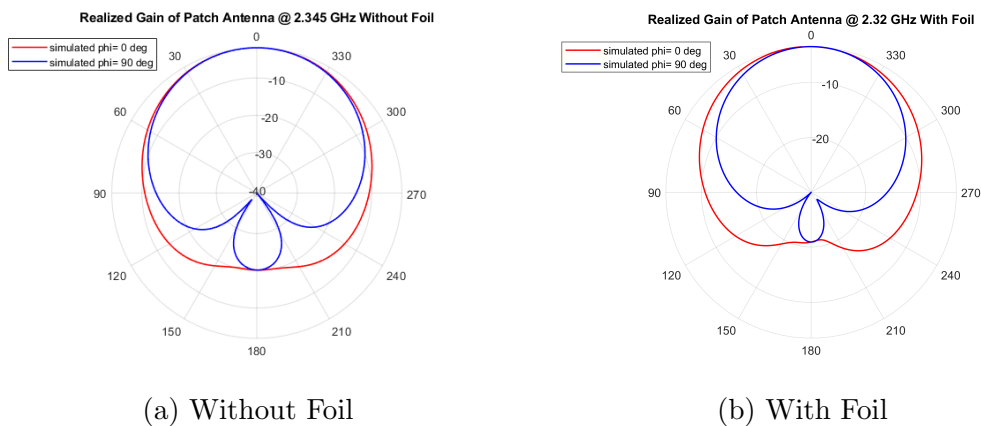


Figure 4.10: S11 of the Simulated Antenna With and Without Foil



(a) Without Foil

(b) With Foil

Figure 4.11: Gain of the simulated antenna with and without foil.



The number of actuators and their position on the vibrating plate are an importing factor in determining the modal shapes of the plate. Therefore, we should rely on a preliminary vibration analysis before deciding on the final design. For this purpose, a harmonic response study is implemented on ANSYS Workbench. A simplified representation of this analysis is shown in Figure 4.12, where the plate has more realistic boundary conditions and many possible positions to place the actuators. The results of two configurations with different actuator placements is presented in figure 4.14. Although we can notice different shapes for each configuration at a certain frequency, figure 4.13 indicates that the frequency response of these two configurations over the frequency range [5-1000 Hz] is similar. In other words, both configurations attain high displacement amplitude values over similar frequency ranges. However, it is important to note that these two configurations are only two examples of a wide variety of possible combinations of boundary conditions and actuators positions. Further analyses are needed before deciding on the best configuration.

Finally, to check if the simulation would match the experimental results, we performed a simulation on the vibration exciter setup. Figure 4.15 shows similar shapes for certain frequencies to those obtained in figure 4.2; however, with a small shift in frequency, which might be due to the weight of the powder.

As an additional step, different shapes for the vibrating plate were simulated on Workbench. Moreover, the effect of offsetting the support was also studied. The investigated profiles are:

- Circular.
- Hexagonal.
- Pentagonal.
- Rectangular.

- Square.
- Triangular.

Figure 4.16 shows the results of some of the simulated shapes. It can be noticed that offsetting the support from the center of the plate results in asymmetric shapes, which could be useful for our antenna application. Therefore, these shapes were converted to CAD models, as seen in figure 4.17. Then, they were imported to HFSS for simulation, as shown in figure 4.18. The results in figure 4.19 indicate a change in radiation pattern, in addition to a beam steering capability. As for S11 response, plotted in figure 4.20, we can notice an enhancement in the impedance bandwidth from shape 1, to shape 2 and shape 3.

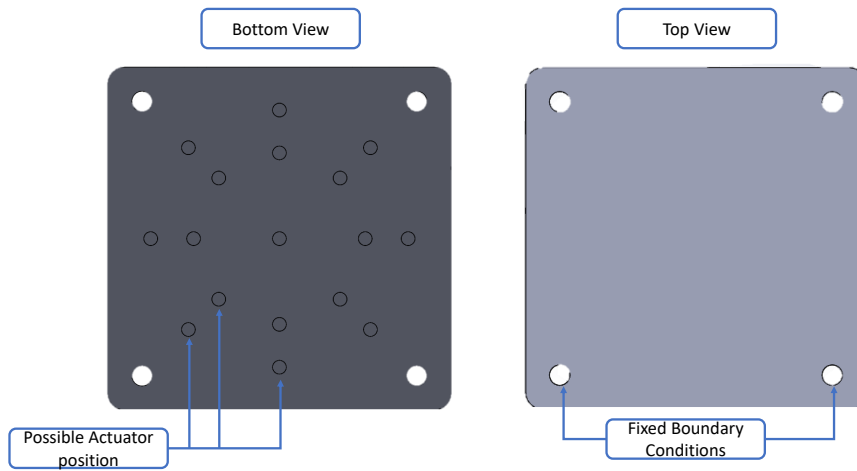


Figure 4.12: FR4 plate model for harmonic response simulations.

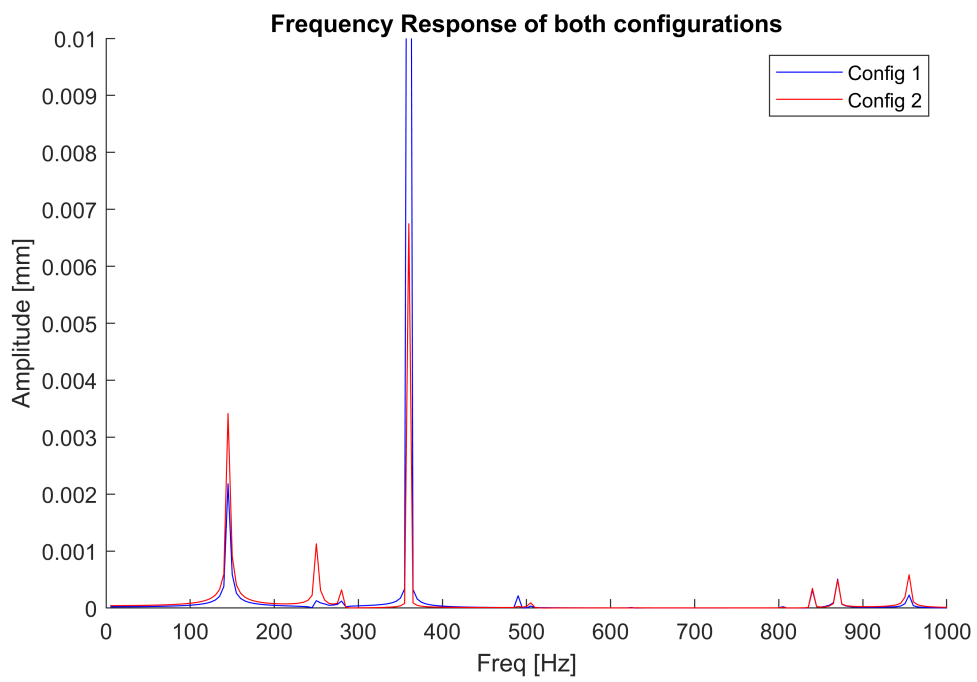
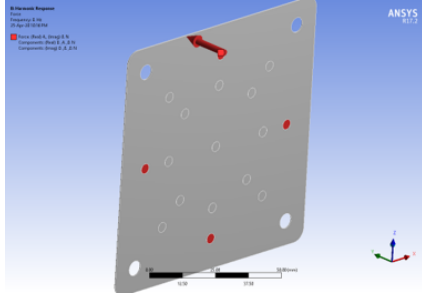
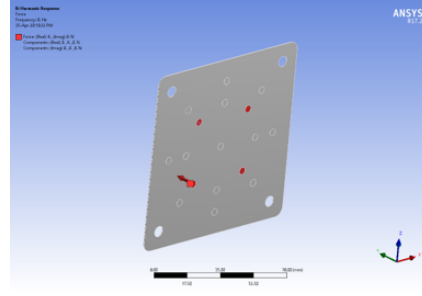


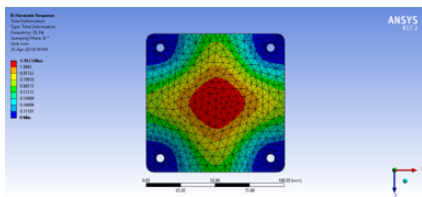
Figure 4.13: Frequency response of two actuator configurations.



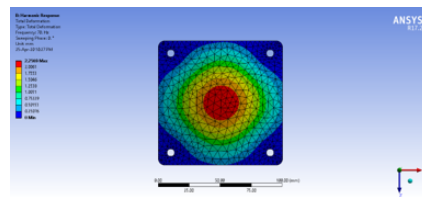
(a) Actuators Placement for 1st config



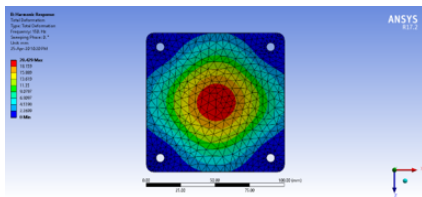
(b) Actuators Placement for 2nd config



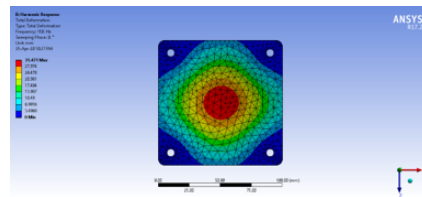
(c) 70 Hz



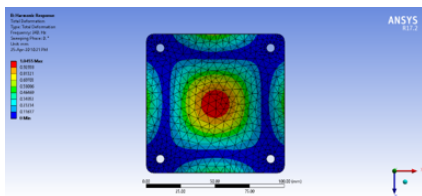
(d) 70 Hz



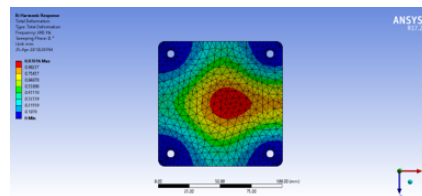
(e) 150 Hz



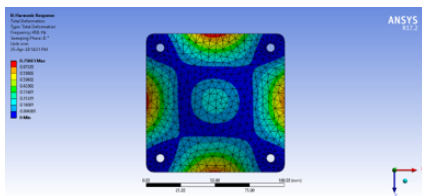
(f) 150 Hz



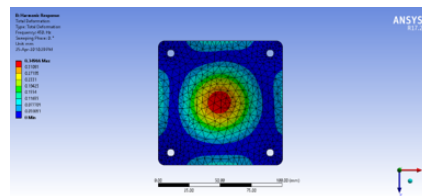
(g) 240 Hz



(h) 240 Hz

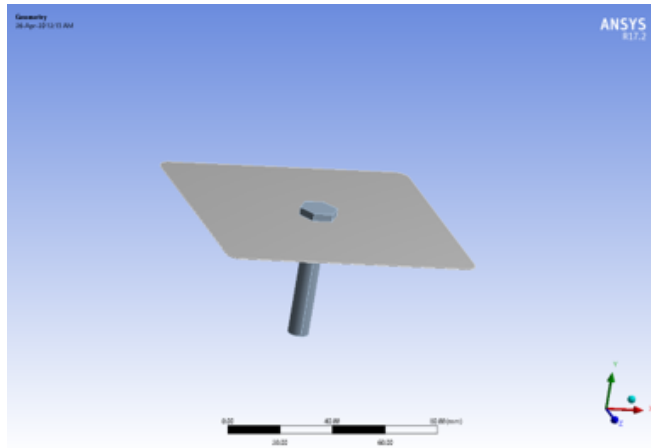


(i) 450 Hz

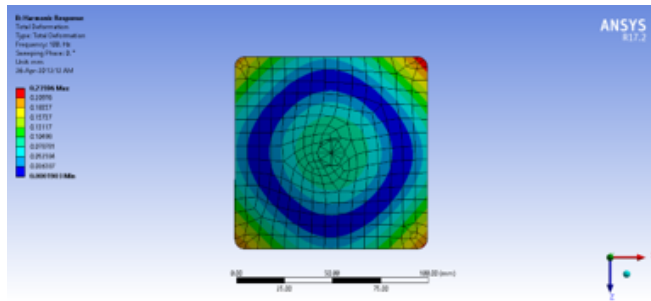


(j) 450 Hz

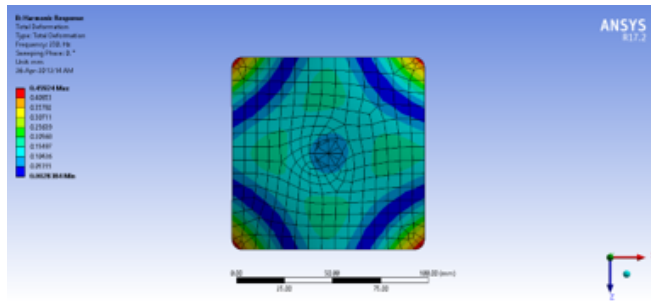
Figure 4.14: Modal shapes comparison for two different actuator placement



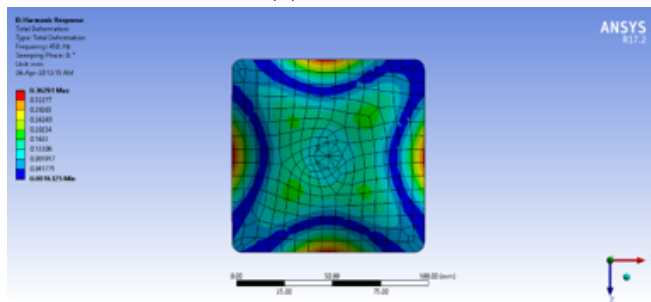
(a) Simulated Plate and Bolt Geometry



(b) 100 Hz

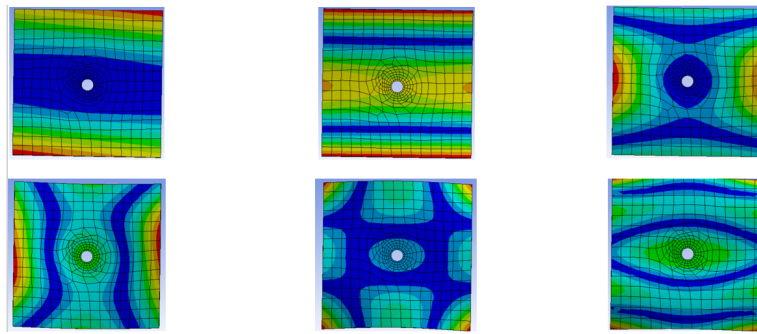


(c) 230 Hz

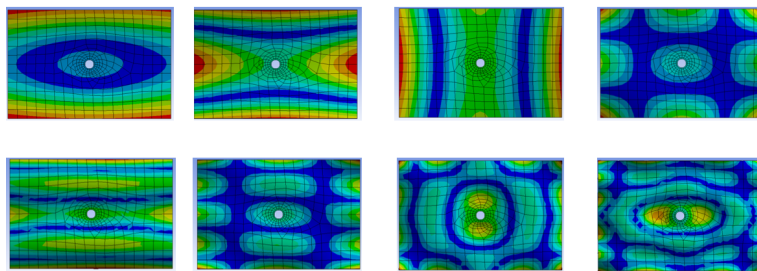


(d) 450 Hz

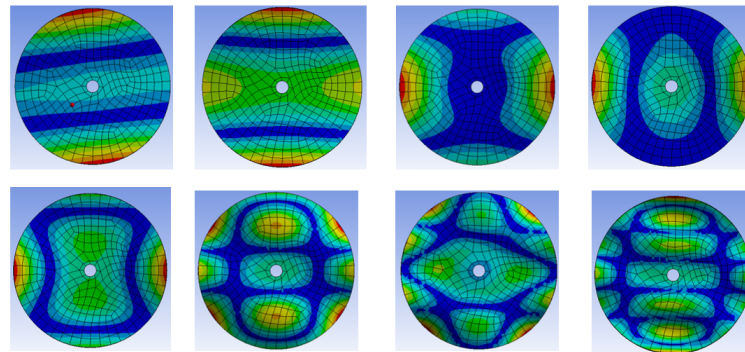
Figure 4.15: Harmonic response simulation of the plate on the vibration exciter setup.



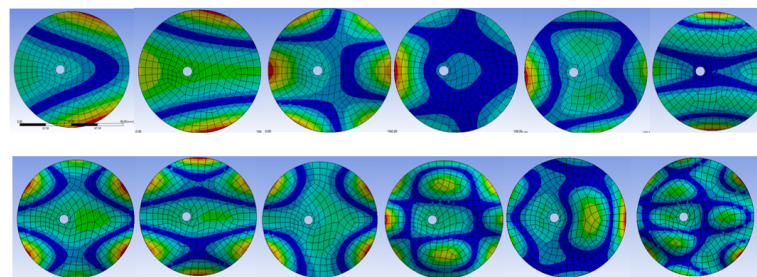
(a) Square profile



(b) Rectangular profile



(c) Circular profile



(d) Offset-support circular profile

Figure 4.16: Harmonic response simulation of the different plate shapes.

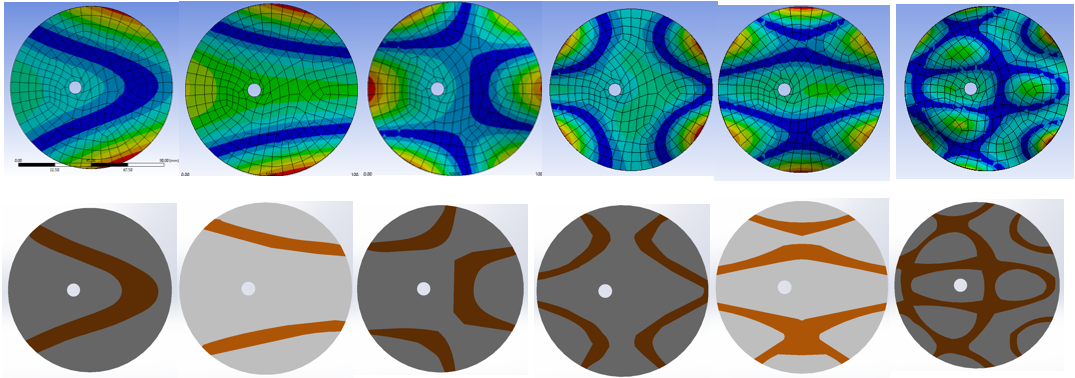


Figure 4.17: Frequency response of two actuator configurations.

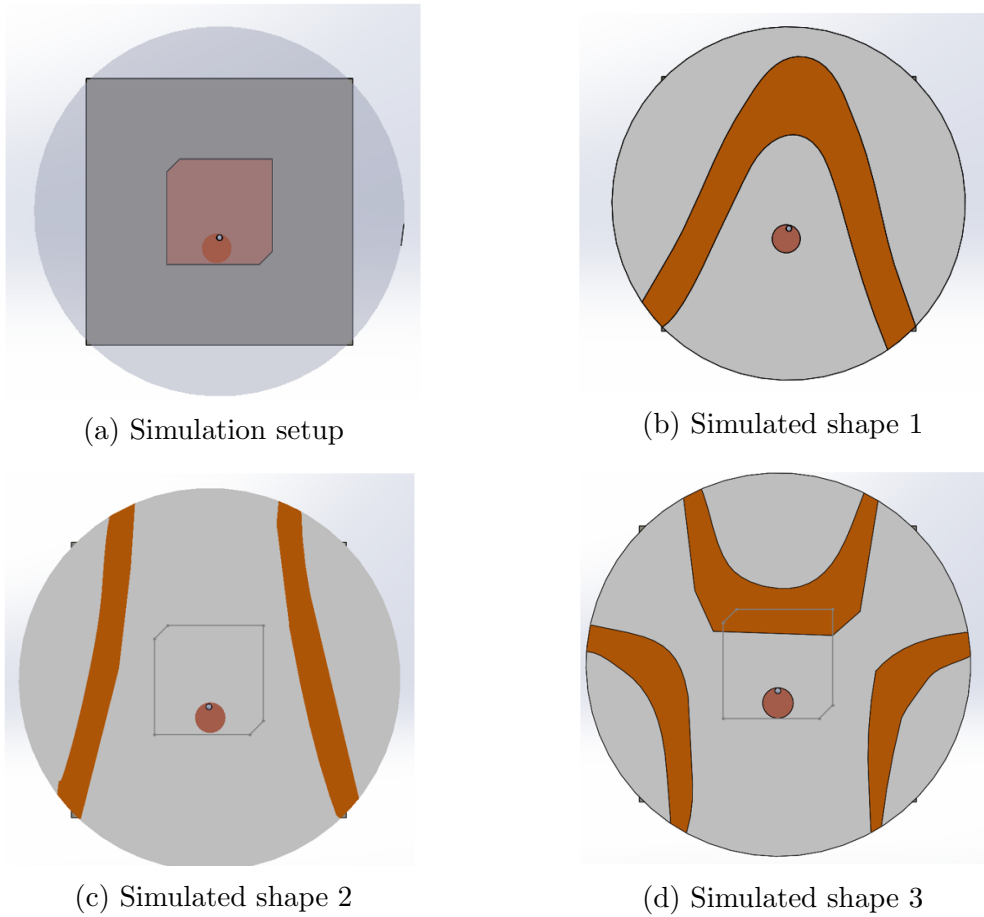
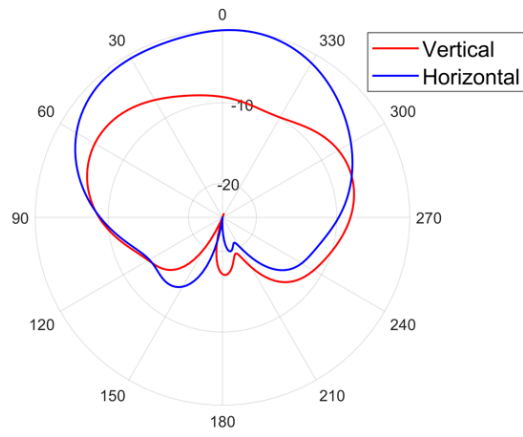
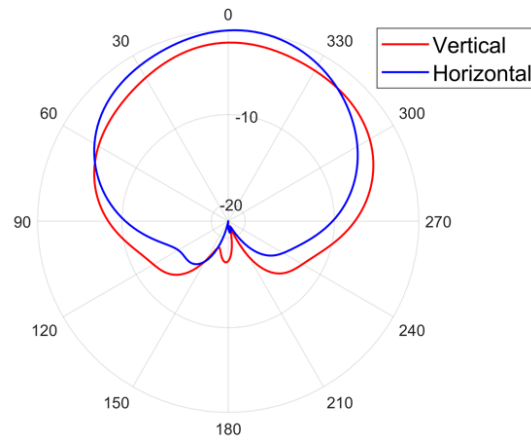


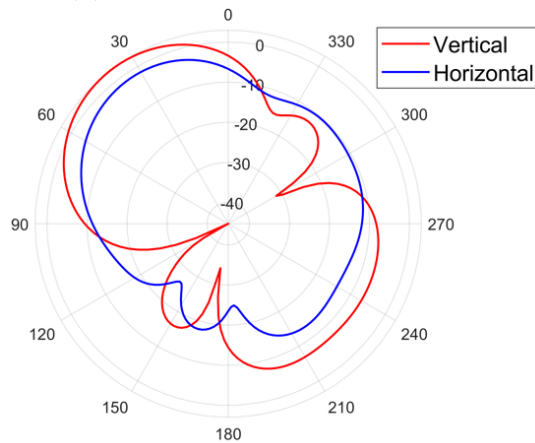
Figure 4.18: Simulated offset shapes of circular plates.



(a) Radiation pattern of shape 1



(b) Radiation pattern of shape 2



(c) Radiation pattern of shape 2

Figure 4.19: Radiation patterns of the simulated offset shapes.



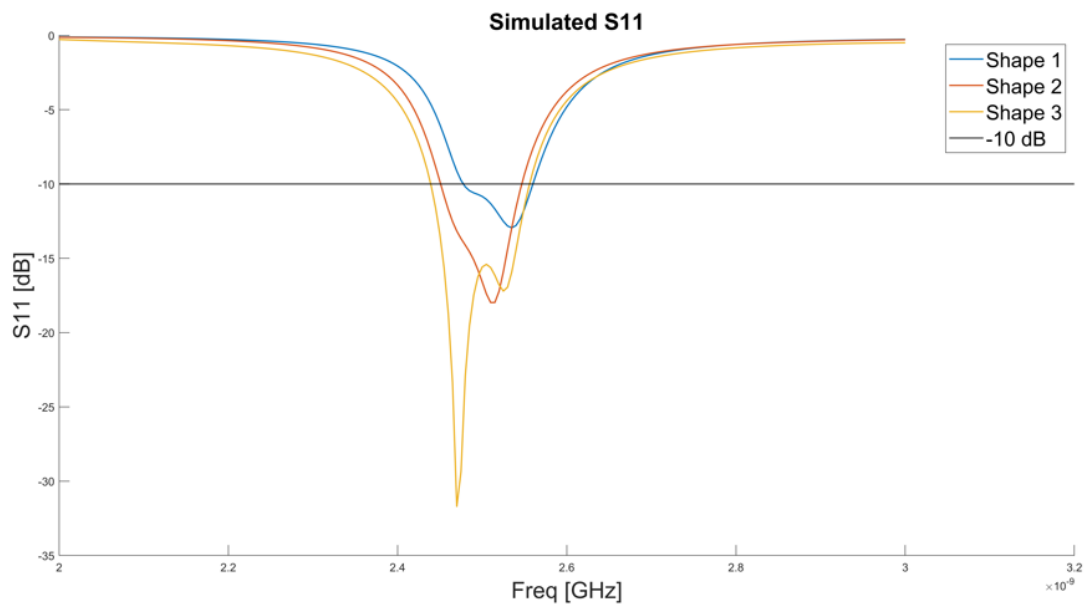


Figure 4.20: S11 plot of the simulated offset shapes.

# Chapter 5

## Future Work

### 5.1 Moiré Patterns Antenna

For future prototypes, several improvements can be achieved. First, the design of the moiré patch's rotation should be improved to minimize friction. Second, the SMA wire size, length, and shape should be optimized to reduce the energy expenditure of the device. The power consumption can also be reduced by replacing one of the SMA spring by an elastic band, acting as a bias for the SMA spring. Finally, the effect of other moiré pattern shapes on the antenna's characteristic should be investigated. In parallel, the driven antenna can be replaced by another types of patch antennas, with different dimensions and different frequency bands, in addition to trying the moiré effect on an antenna array.

### 5.2 Chladni Patterns Antenna

Since the design of this antenna is still at an early stage, it requires more simulations and experiments. One of the main design decision is choosing

the appropriate actuator. Since each type of the haptic actuators has its own drawback, the final actuator choice will have a significant impact on the excitation frequencies and the obtained shapes. These shapes can also be optimized by changing the location of the supports on the vibrating plate. Another important aspect to consider is the design of the supporting structure, since its role includes the preservation of the conductive grains on the vibrating plate, in addition to the need of a mechanism to conserve the formed shape by applying a small pressure on the grain, as this will also enhance the conductivity of the grains.

# Bibliography

- [1] C. A. Balanis, *Antenna theory: analysis and design*. John Wiley & sons, 2016.
- [2] M. Dhillon and S. Kumar, “Performance analysis and comparison of various rectenna based rf energy harvesting systems,”
- [3] N. Singh, M. Sharma, and A. Verma, “Antenna and its application,” vol. 6, pp. 95–97, 01 2015.
- [4] J. Sankar, “Antenna polarisation,” Jun 2017.
- [5] J.-M. Hannula, J. Holopainen, and V. Viikari, “Concept for frequency-reconfigurable antenna based on distributed transceivers,” *IEEE Antennas and Wireless Propagation Letters*, vol. 16, pp. 764–767, 2016.
- [6] R. L. Haupt and M. Lanagan, “Reconfigurable antennas,” *IEEE Antennas and Propagation Magazine*, vol. 55, no. 1, pp. 49–61, 2013.
- [7] B. Liu, J. Qiu, S. Lan, N. Wang, and H. Liu, “Bandwidth reconfigurable cylindrical dielectric resonator antenna excited by double-ring slot,” in *2018 IEEE International Symposium on Antennas and Propagation & USNC/URSI National Radio Science Meeting*, pp. 2097–2098, IEEE, 2018.

- [8] H. L. Zhu, S. W. Cheung, and T. I. Yuk, “Mechanically pattern reconfigurable antenna using metasurface,” *IET Microwaves, Antennas & Propagation*, vol. 9, no. 12, pp. 1331–1336, 2015.
- [9] H. Friis, C. Feldman, and W. Sharpless, “The determination of the direction of arrival of short radio waves,” *Proceedings of the Institute of Radio Engineers*, vol. 22, no. 1, pp. 47–78, 1934.
- [10] X. Liu, C. L. Zekios, and S. V. Georgakopoulos, “Analysis of a packable and tunable origami multi-radii helical antenna,” *IEEE Access*, vol. 7, pp. 13003–13014, 2019.
- [11] Y. Tawk, “Physically controlled cubesat antennas with an adaptive frequency operation,” *IEEE Antennas and Wireless Propagation Letters*, vol. 18, no. 9, pp. 1892–1896, 2019.
- [12] L. H. Blumenschein, L. T. Gan, J. A. Fan, A. M. Okamura, and E. W. Hawkes, “A tip-extending soft robot enables reconfigurable and deployable antennas,” *IEEE Robotics and Automation Letters*, vol. 3, no. 2, pp. 949–956, 2018.
- [13] I. T. Nassar, H. Tsang, D. Bardroff, C. P. Lusk, and T. M. Weller, “Mechanically reconfigurable, dual-band slot dipole antennas,” *IEEE Transactions on Antennas and Propagation*, vol. 63, no. 7, pp. 3267–3271, 2015.
- [14] J. M. Floc’h and I. B. Trad, “Design of mechanically reconfigurable meander antenna using the galinstan liquid metal,” 2017.
- [15] H. Zhu, X. Liu, S. Cheung, and T. Yuk, “Frequency-reconfigurable antenna using metasurface,” *IEEE Transactions on Antennas and Propagation*, vol. 62, no. 1, pp. 80–85, 2013.

- [16] D. Rodrigo, L. Jofre, and B. A. Cetiner, “Circular beam-steering reconfigurable antenna with liquid metal parasitics,” *IEEE transactions on antennas and propagation*, vol. 60, no. 4, pp. 1796–1802, 2012.
- [17] A. Mehdipour, T. A. Denidni, A.-R. Sebak, C. W. Trueman, I. D. Rosca, and S. V. Hoa, “Mechanically reconfigurable antennas using an anisotropic carbon-fibre composite ground,” *IET Microwaves, Antennas & Propagation*, vol. 7, no. 13, pp. 1055–1063, 2013.
- [18] A. Boukarkar, X. Q. Lin, Y. Jiang, Y. J. Chen, L. Y. Nie, and P. Mei, “Compact mechanically frequency and pattern reconfigurable patch antenna,” *IET Microwaves, Antennas & Propagation*, vol. 12, no. 11, pp. 1864–1869, 2018.
- [19] I. T. McMichael, “A mechanically reconfigurable patch antenna with polarization diversity,” *IEEE Antennas and Wireless Propagation Letters*, vol. 17, no. 7, pp. 1186–1189, 2018.
- [20] R. Pereira, R. Gillard, R. Sauleau, P. Potier, T. Dousset, and X. Delestre, “Dual linearly-polarized unit-cells with nearly 2-bit resolution for reflectarray applications in x-band,” *IEEE Transactions on Antennas and Propagation*, vol. 60, no. 12, pp. 6042–6048, 2012.
- [21] H. F. Abutarboush, R. Nilavalan, S. Cheung, K. M. Nasr, T. Peter, D. Budimir, and H. Al-Raweshidy, “A reconfigurable wideband and multi-band antenna using dual-patch elements for compact wireless devices,” *IEEE transactions on antennas and propagation*, vol. 60, no. 1, pp. 36–43, 2011.
- [22] M. Riel and J.-J. Laurin, “Design of an electronically beam scanning reflectarray using aperture-coupled elements,” *IEEE Transactions on Antennas and Propagation*, vol. 55, no. 5, pp. 1260–1266, 2007.

- [23] M. A. Forman and Z. B. Popovic, "A tunable second-resonance cross-slot antenna," in *IEEE Antennas and Propagation Society International Symposium 1997. Digest*, vol. 1, pp. 18–21, IEEE, 1997.
- [24] P.-L. Chi, R. Waterhouse, and T. Itoh, "Compact and tunable slot-loop antenna," *IEEE transactions on antennas and propagation*, vol. 59, no. 4, pp. 1394–1397, 2011.
- [25] T. Debogovic and J. Perruisseau-Carrier, "Low loss mems-reconfigurable 1-bit reflectarray cell with dual-linear polarization," *IEEE Transactions on Antennas and Propagation*, vol. 62, no. 10, pp. 5055–5060, 2014.
- [26] J. M. Kovitz, H. Rajagopalan, and Y. Rahmat-Samii, "Design and implementation of broadband mems rhcp/lhcp reconfigurable arrays using rotated e-shaped patch elements," *IEEE Transactions on Antennas and Propagation*, vol. 63, no. 6, pp. 2497–2507, 2015.
- [27] B. Majumder, K. Krishnamoorthy, J. Mukherjee, and K. Ray, "Frequency-reconfigurable slot antenna enabled by thin anisotropic double layer metasurfaces," *IEEE Transactions on Antennas and Propagation*, vol. 64, no. 4, pp. 1218–1225, 2016.
- [28] Y. Tawk, J. Costantine, F. Ayoub, C. Christodoulou, D. Doyle, and S. Lane, "Physically reconfigurable antennas: Concepts and automation," in *2017 IEEE International Symposium on Antennas and Propagation & USNC/URSI National Radio Science Meeting*, pp. 419–420, IEEE, 2017.
- [29] I. T. Nassar, T. M. Weller, and C. P. Lusk, "Radiating shape-shifting surface based on a planar hoberman mechanism," *IEEE transactions on antennas and propagation*, vol. 61, no. 5, pp. 2861–2864, 2013.

- [30] X. Yang, S. Xu, F. Yang, M. Li, H. Fang, Y. Hou, S. Jiang, and L. Liu, “A mechanically reconfigurable reflectarray with slotted patches of tunable height,” *IEEE Antennas and Wireless Propagation Letters*, vol. 17, no. 4, pp. 555–558, 2018.
- [31] S. J. Mazlouman, A. Mahanfar, C. Menon, and R. G. Vaughan, “Reconfigurable axial-mode helix antennas using shape memory alloys,” *IEEE Transactions on Antennas and Propagation*, vol. 59, no. 4, pp. 1070–1077, 2011.
- [32] I. Amidror, *The theory of the Moiré phenomenon: Volume I: Periodic layers*, vol. 38. Springer Science & Business Media, 2009.
- [33] E. Gabrielyan, “The basics of line moiré patterns and optical speedup,” *arXiv preprint physics/0703098*, 2007.
- [34] F.-P. Chiang, “Moiré methods of strain analysis,” *Experimental mechanics*, vol. 19, no. 8, pp. 290–308, 1979.
- [35] V. J. Cadarso, S. Chosson, K. Sidler, R. D. Hersch, and J. Brugger, “High-resolution 1d moirés as counterfeit security features,” *Light: Science & Applications*, vol. 2, no. 7, pp. e86–e86, 2013.
- [36] *Shape Memory Alloys*, ch. 6, pp. 298–345. John Wiley Sons, Ltd, 2007.
- [37] J. Arias Guadalupe, D. Copaci, D. Serrano del Cerro, L. Moreno, and D. Blanco, “Efficiency analysis of sma-based actuators: Possibilities of configuration according to the application,” *Actuators*, vol. 10, no. 3, 2021.
- [38] J. Mohd Jani, “Design optimisation of shape memory alloy linear actuator applications.”



- [39] S. H. Mahdavi and P. Bentley, “Evolving noise tolerant antenna configurations using shape memory alloys,” 2004.
- [40] P. Motzki, “Efficient sma actuation—design and control concepts,” *Proceedings*, vol. 64, no. 1, 2020.
- [41] S. Chakraverty, *Vibration of plates*. CRC press, 2008.
- [42] J. Beament, *How We Hear Music: The Relationship between Music and the Hearing Mechanism*. Boydell amp; Brewer, 2002.
- [43] R. Porter, “Eigenfrequencies and eigenmodes for a thin rectangular elastic plate with free edges,” in *British Applied Mathematics Colloquium, Guildford, England*, vol. 6, 2017.
- [44] E. F. F. Chladni, *Entdeckungen über die Theorie des Klanges*. Zentralantiquariat der DDR, 1787.
- [45] P. Tuan, Y. Lai, C. Wen, K.-F. Huang, and Y.-F. Chen, “Point-driven modern chladni figures with symmetry breaking,” *Scientific reports*, vol. 8, no. 1, pp. 1–13, 2018.
- [46] K. Mori, A. Watanabe, Y. Okai, and M. Saito, “Conductivity of copper powders with and without surface treatment,” *Powder technology*, vol. 59, no. 3, pp. 191–197, 1989.
- [47] Y. P. Mamunya, H. Zois, L. Apekis, and E. Lebedev, “Influence of pressure on the electrical conductivity of metal powders used as fillers in polymer composites,” *Powder Technology*, vol. 140, no. 1-2, pp. 49–55, 2004.
- [48] M. Zanon, M. Nassuato, I. Rampin, J. Echeberria, and A. M. Martinez, “The conductive behavior of copper and silver-coated copper powders,”

- [49] F. Wang, “Haptic energy consumption,” 2014.
- [50] “Dualshock 4 controller rumble motors replacement,” May 2018.
- [51] G. Poetsch, “Everything you ever wanted to know about core haptics,” Nov 2019.
- [52] PIEZO.COM, “Introduction to piezos,” 2018.
- [53] D. Petrov, “Here’s how note 10 may use sound on display tech to get an ‘all-screen’ design,” Jul 2019.

